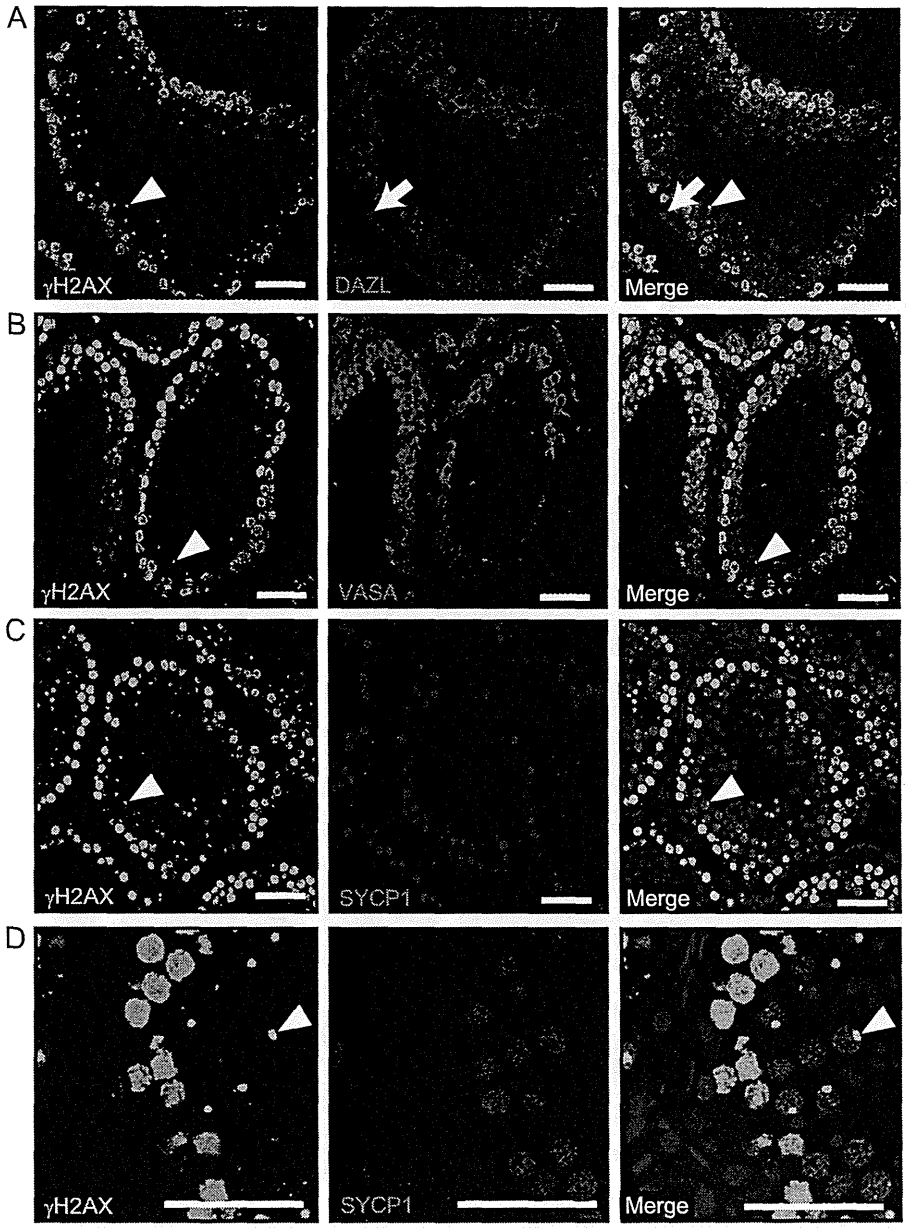

Fig. 4. Meiosis-associated formation of XY body and synaptonemal complex in the adult spermatocytes. Confocal images of adult marmoset testis sections co-stained with antibodies against germ cell and meiotic nuclear markers, including (A) anti-γH2AX and anti-DAZL antibodies, (B) anti-γH2AX and anti-VASA antibodies, and (C, D) anti-γH2AX and anti-SYCP1 antibodies. (D) A higher magnification of (C) clearly displays the formation of the XY body and synaptonemal complex in the nuclei of pachytene spermatocytes. Arrowheads indicate the XY body with confined sublocalization of γH2AX protein. In the image of (A), an arrow indicates $DAZL^{+}\gamma H2AX^{-}$ spermatogonia. Nuclei were counterstained with Hoechst 33342. Scale bar, 50 μm.

but are consistently degenerated in the central part of seminiferous tubules (Li et al., 2005). Therefore, we next moved on to characterize the juvenile marmoset testis, particularly focusing on the pre-spermatogonia. According to our previous study, DAZL and VASA proteins were expressed in the pre-spermatogonia in 10-month juvenile marmoset testes whereas spermatogonia adjacent to the basement membrane expressed DAZL but not VASA protein (Fig. 5A and B). Surprisingly, the pre-spermatogonia also expressed MARWI protein, which in the adult was observed in the pachytene spermatocytes and onward (Fig. 3). Neither quiescent (SALL4) nor dividing spermatogonia (Ki67) markers were expressed in the $MARWI^{+}$ pre-spermatogonia (Fig. 5C and D). Nevertheless, we sometimes found the pre-spermatogonia expressing SALL4 and C-KIT proteins (Fig. 5E) but they were negative for MARWI protein (Fig. 5C). These observations implied that the pre-spermatogonia might be a cell population that escapes from the normal commitment to a spermatogonial cell fate.

Then, we examined the expression of other meiosis-associated genes in the pre-spermatogonia. The $MARWI^{+}$ pre-spermatogonia indeed expressed CLGN and RanBPM proteins (Fig. 6A and B), but the subcellular localization of RanBPM protein was confined to the cytoplasm unlike the nucleocytoplasmic localization observed in adults (Fig. 3D). We further investigated the meiotic nuclear structures based on the expression of γH2AX and SYCP1 proteins. Again, γH2AX was present in the $VASA^{+}$ pre-spermatogonia (Fig. 6C–E). The nuclear distribution was primarily punctate (Fig. 6C) and only a few pre-spermatogonia exhibited the formation of an XY body (Fig. 6D). This was also the case in another juvenile marmoset testis with a slightly

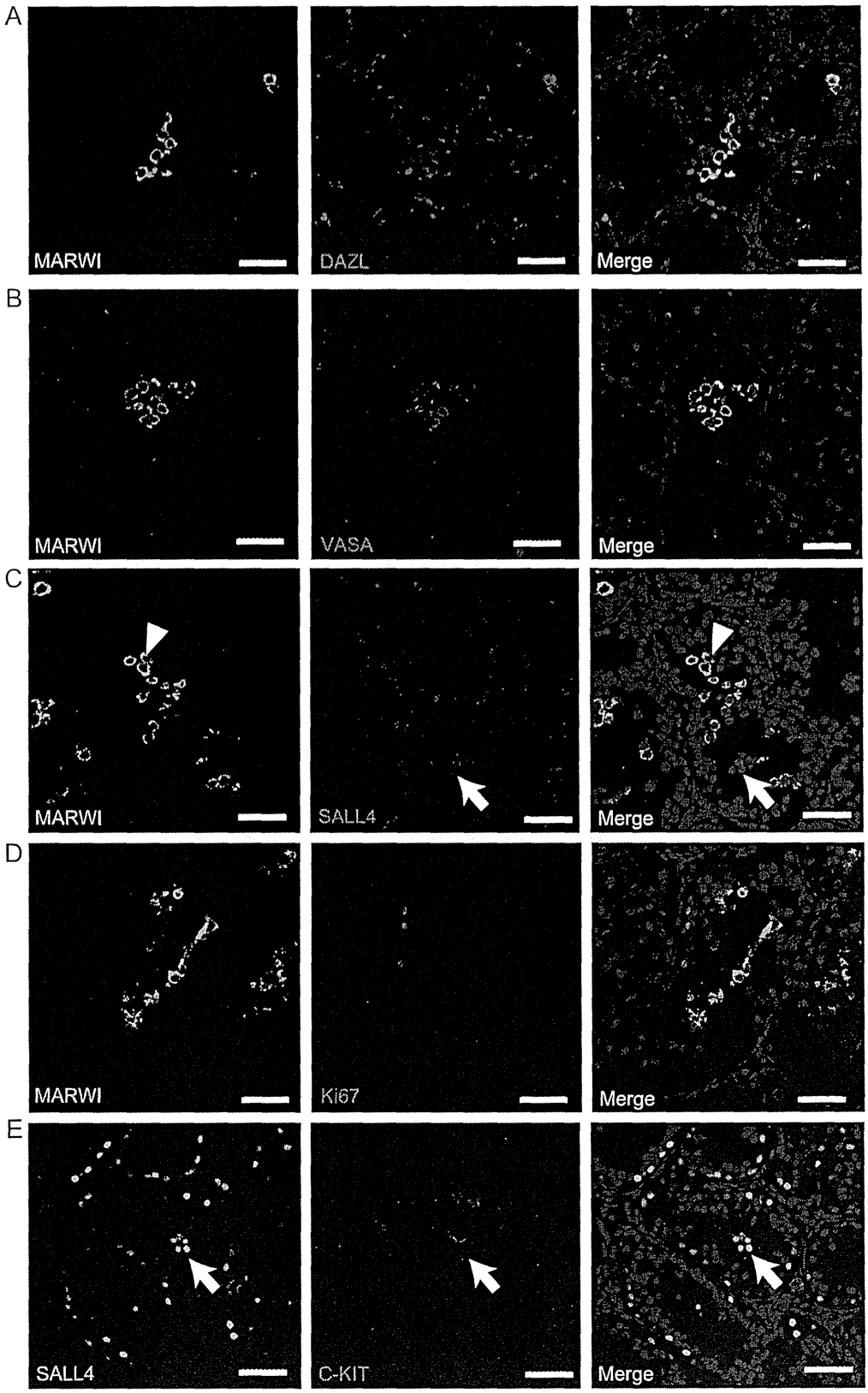

Fig. 5. Premature expression of MARWI protein in the pre-spermatogonia of juvenile marmosets. Confocal images of juvenile marmoset testis sections co-stained with (A) anti-MARWI and anti-DAZL antibodies, (B) anti-MARWI and anti-VASA antibodies, (C) anti-MARWI and anti-SALL4 antibodies, (D) anti-MARWI and anti-Ki67 antibodies, and (E) anti-SALL4 and anti-C-KIT antibodies. (C) SALL4 protein was observed in some pre-spermatogonia as well as spermatogonia population present on the basement membrane. The *SALL4*$^{+}$ *pre-spermatogonia were negative for* MARWI *(arrow) and vice versa (arrowhead).* (E) *A few pre-spermatogonia expressed both* SALL4 *and* C-KIT proteins (arrow), while, in spermatogonia, these proteins were expressed in exclusive cell populations. Nuclei were counterstained with Hoechst 33342. Scale bar, 50 μm.

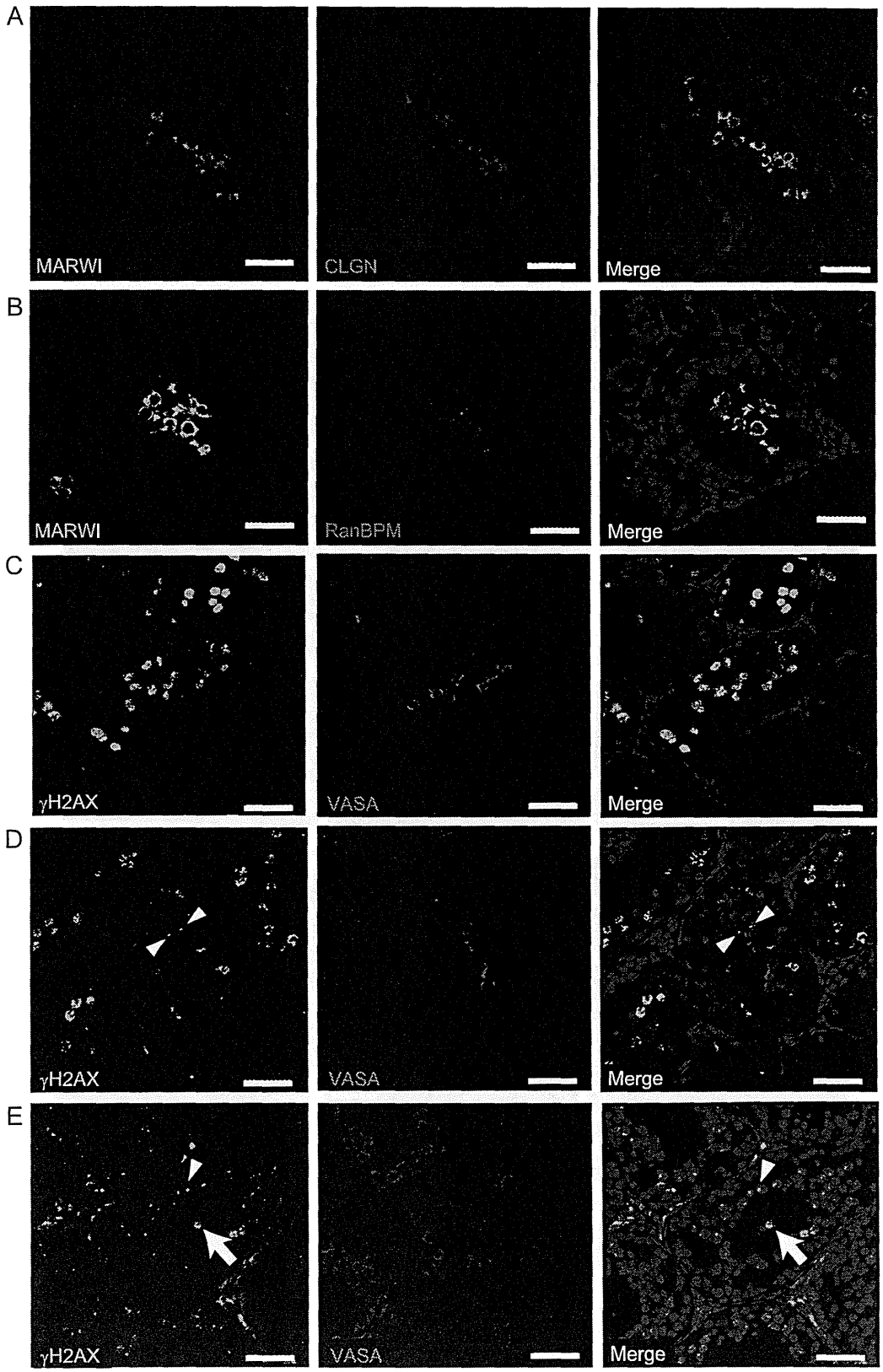

Fig. 6. Expression of meiotic markers in the pre-spermatogonia of juvenile marmosets. Confocal images of juvenile marmoset testis sections co-stained with antibodies against meiosis-associated proteins, including (A) anti-MARWI and anti-CLGN antibodies, (B) anti-MARWI and anti-RanBPM antibodies, and (C–E) anti-γH2AX and anti-VASA antibodies. (D) In a few seminiferous tubules, the VASA^{+} pre-spermatogonia exhibited a γH2AX signal in the form of the XY body (arrowhead). (E) In the slightly mature juvenile testis, very few pre-spermatogonia remained, expressing VASA protein and γH2AX with the punctate nuclear distribution (arrow). The newly formed spermatocytes also expressed VASA protein and γH2AX but in the form of the XY body (arrowhead). Nuclei were counterstained with Hoechst 33342. Scale bar, 50 μm.

mature appearance, in which the number of the pre-spermatogonia had decreased (Fig. 6E). In the nuclei of the pre-spermatogonia, SYCP1 protein was also detectable in the form of a synaptonemal complex (Fig. 7A and B) but the abundance seemed much lower compared with adult spermatocytes (Fig. 4C and D). Additionally, in the juvenile testis of another marmoset with a slightly mature appearance, the synaptonemal complex seemed to be deformed in association with abnormal cellular and nuclear morphologies (Fig. 7C and D).

The pre-spermatogonia in juvenile marmoset testis undergo apoptosis

Given the observation of the degrading nuclear structure and cell morphology, we assumed that the pre-spermatogonia in juvenile testis might result in apoptosis. We therefore investigated apoptosis markers in the pre-spermatogonia, and found that activated Caspase3 (Said et al., 2004) was present in the pre-spermatogonia (Fig. 8A) and became predominant according to testicular development (Fig. 8B). The activated caspase3 was also observed in the spermatocytes derived from spermatogonia (Fig. 8B). We subsequently examined the cleavage form of PARP1, a target protein of activated Caspase3 in

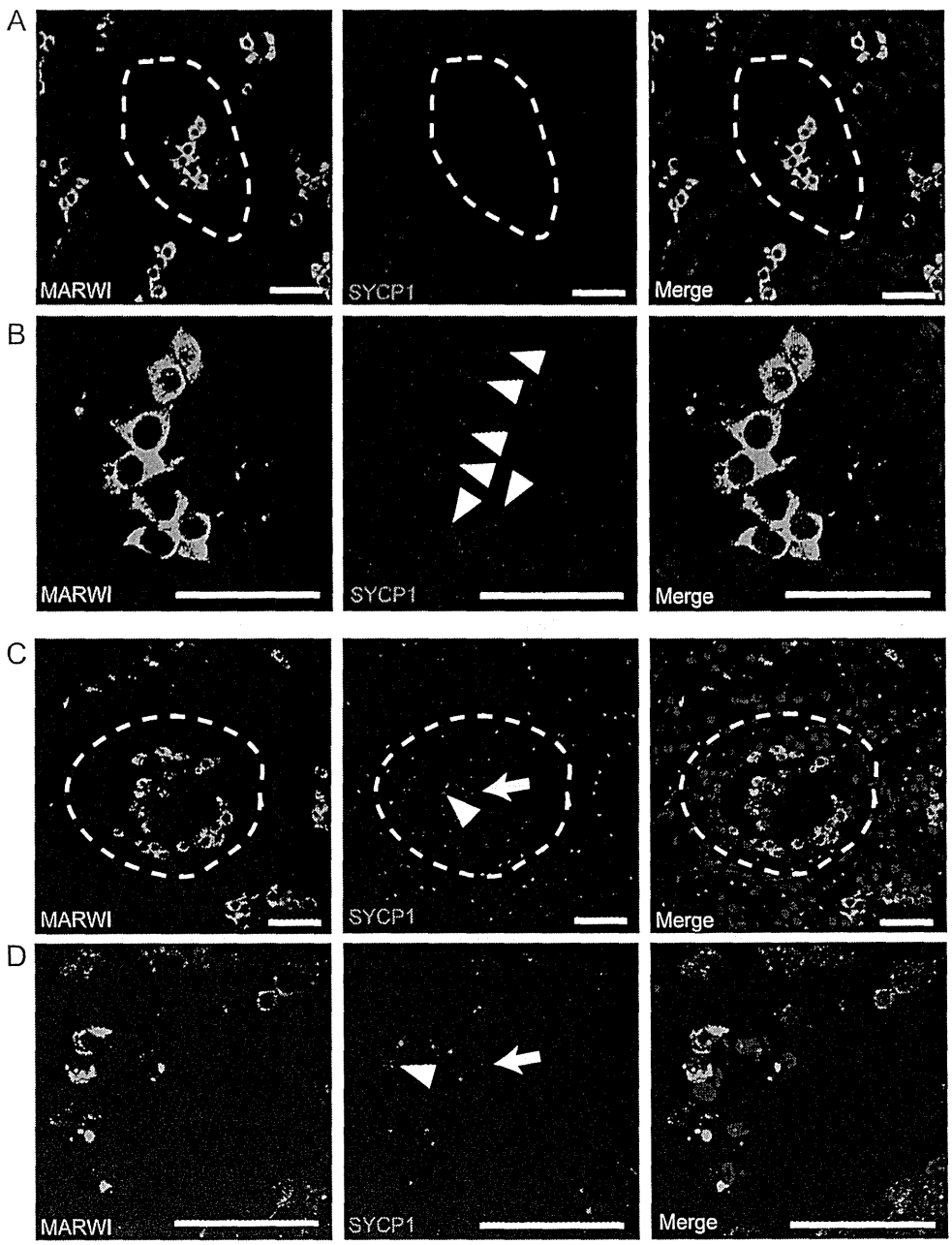

Fig. 7. Degeneration of synaptonemal complex in the pre-spermatogonia of juvenile marmosets. Confocal images of juvenile marmoset testis sections co-stained with anti-MARWI and anti-SYCP1 antibodies. (A, B) Immature juvenile testis. (B) A higher magnification of (A). Synaptonemal complex-like structures could be seen in the nucleus of the MARWI$^+$ pre-spermatogonia (arrowhead) although the signal intensity was weaker than that observed in adult spermatocytes. (C, D) Juvenile marmoset testis with slightly mature appearance. (D) A higher magnification of (C). Some pre-spermatogonia formed synaptonemal complexes (arrowhead) while the others exhibited degenerated structures (arrow). Nuclei were counterstained with Hoechst 33342. Scale bar, 50 μm.

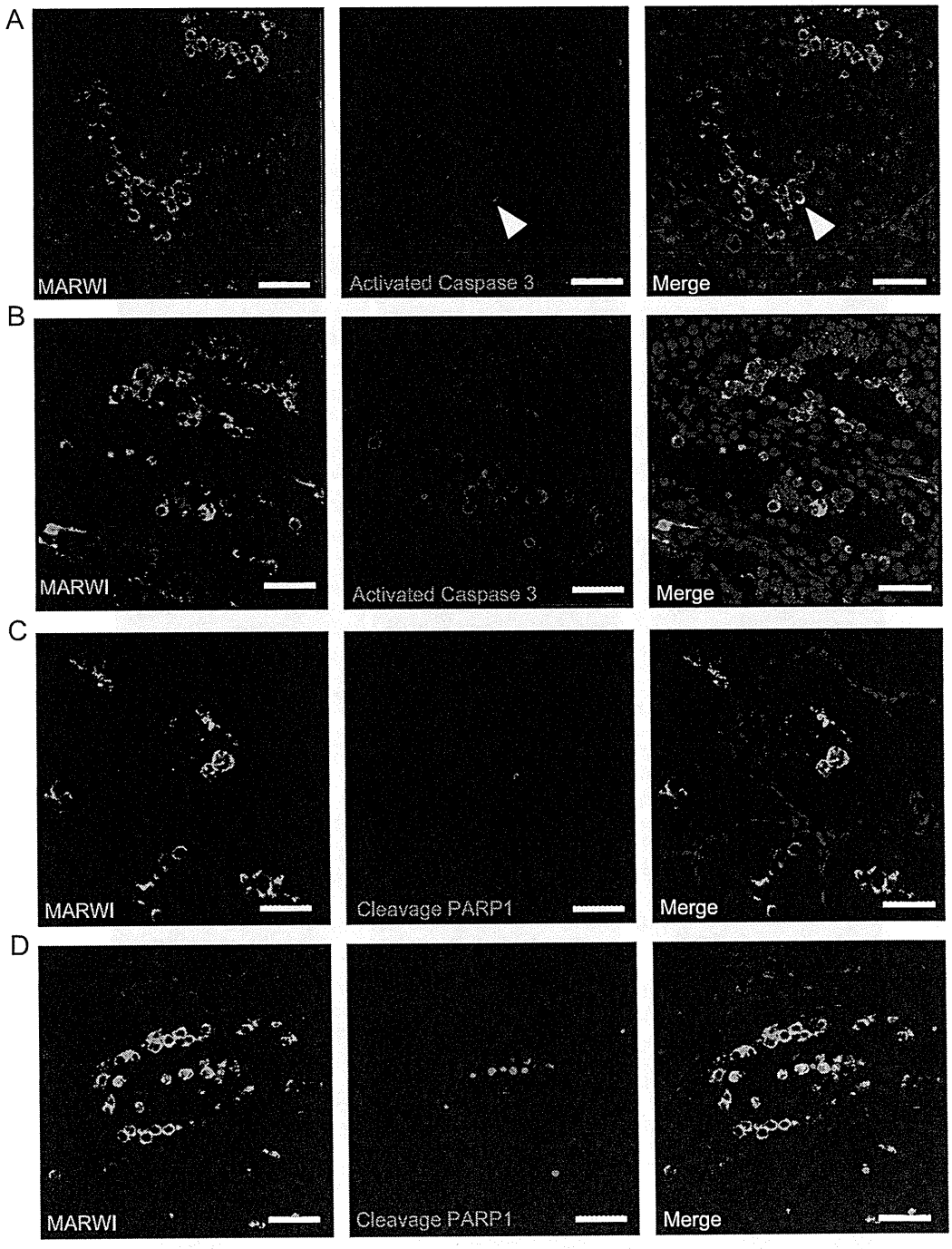

Fig. 8. Apoptotic markers in the pre-spermatogonia of juvenile marmosets. Confocal images of juvenile marmoset testis sections co-stained with antibodies against germ cell and apoptotic markers, including (A, B) anti-MARWI and anti-activated Caspase3 antibodies, and (C, D) anti-MARWI and anti-cleavage PARP1 antibodies. (A) In immature juvenile testis, a few pre-spermatogonia exhibited an activated Caspase3 signal (arrowhead). (B) Almost all of the pre-spermatogonia became positive for activated Caspase3 in juvenile testis with a slightly mature appearance. (C) In the immature juvenile testes, cleavage PARP1 was present in very few pre-spermatogonia. (D) In the juvenile testis with a slightly mature appearance, cleavage PARP1 was present in almost all of the pre-spermatogonia. Nuclei were counterstained with Hoechst 33342. Scale bar, 50 μm.

an apoptotic pathway (YDBIOl6681Agarwal et al., 2009; D'Amours et al., 2001). A small number of pre-spermatogonia were positive for cleavage PARP1 in the less mature juvenile testis, similar to the case of activated caspase3 (Fig. 8C). In contrast, in the juvenile testis with a slightly mature appearance, cleavage PARP1 was frequently observed in the pre-spermatogonia but not in the spermatocytes (Fig. 8D). These data demonstrated that the pre-spermatogonia expressing meiosis-associated genes would be destined to undergo apoptotic cell death eventually.

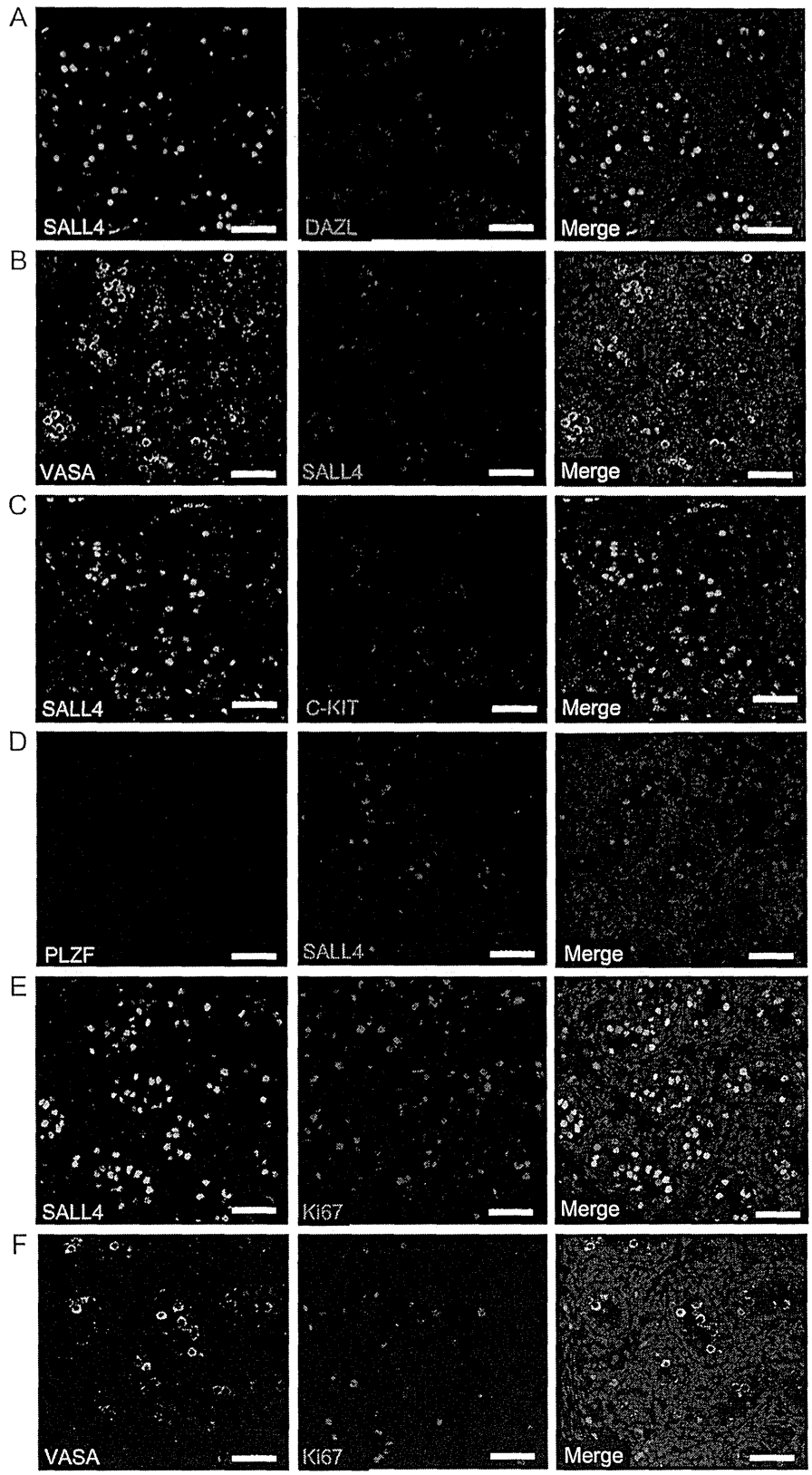

Fig. 9. Expression of germ cell markers in the neonatal gonocytes. Confocal images of neonatal marmoset testis sections co-stained with antibodies against germ cell markers, including (A) anti-*SALL4* and anti-*DAZL* antibodies, (B) anti-*VASA* and anti-*SALL4* antibodies, (C) anti-*SALL4* and anti-*C-KIT* antibodies, (D) anti-PLZF and anti-*SALL4* antibodies, (E) anti-SALL4 and anti-Ki67 antibodies, and (F) anti-VASA and anti-Ki67 antibodies. Nuclei were counterstained with Hoechst 33342. Scale bar, 50 μm.

The gonocyte origin of the pre-spermatogonia in juvenile marmoset testis

To identify whether the pre-spermatogonia in the juvenile testis originate from gonocytes or spermatogonia, we characterized the molecular signature of gonocytes in neonatal marmoset testis. Our previous study revealed that DAZL and VASA proteins were expressed in the marmoset gonocytes (Lin et al., 2012), similar to the pre-spermatogonia in juveniles. We found that the DAZL$^+$ VASA$^+$ gonocytes also expressed SALL4 protein (Fig. 9A and B) unlike the quiescent spermatogonia expressing SALL4 and DAZL but not VASA protein (YDBIOI6681Figs. 1 and 3) (Lin et al., 2012). Furthermore, in contrast to the spermatogonia, SALL4 and C-KIT proteins were co-expressed in the gonocytes (Fig. 9C) whereas the quiescent spermatogonia marker PLZF was absent (Fig. 9D), as is the case in mice (Hobbs et al., 2012). In addition, the SALL4$^+$VASA$^+$ gonocytes were Ki67-negative (Fig. 9E and F) as the neonatal gonocytes are mitotically arrested (YDBIOI6681Culty, 2009, 2013). Taken together, gene expression of gonocytes was very similar to that of the MARWI-negative population of pre-spermatogonia in juveniles (Fig. 5C and E). Considering the present results, the pre-spermatogonia most likely came from the gonocytes, but not spermatogonia, left over in the luminal region of seminiferous tubules during postnatal testicular development, and eventually disappear by apoptosis via a meiosis-like event.

Discussion

Developmental stages of primate spermatogenesis have been defined by classical cellular and nuclear morphologies and testis organization (YDBIOI6681Chemes, 2001; Dreef et al., 2007; Haruyama et al., 2012; Jackson and Edmunds, 1984; Millar et al., 2000; Schlatt and Ehmcke, 2014; Wistuba et al., 2003), while, in mice, the identification of numerous stage-specific marker genes has enabled each developmental process to be identified at a molecular level. By contrast only a limited number of molecular markers are available for primates. To develop our understanding of primate reproductive biology, it is fundamental and indispensable to expand molecular insights of primate spermatogenesis. In this study, we carried out sequential immunofluorescence analyses during postnatal testicular development in the common marmoset to depict a basic molecular atlas of spermatogenesis. Taken all together, we formulated the scenario of gene expression dynamics in germ cells during marmoset testicular development (Fig. 10). We believe that this insight could be essential for understanding primate germ cell development and cell culturing (YDBIOI 6681Imamura et al., 2014, 2012).

According to Clermont's histological classification, primate undifferentiated spermatogonia are defined as two subtypes, mitotically quiescent (reserve) A_{dark} and actively dividing (renewing) A_{pale} spermatogonia (YDBIOI6681Clermont and Antar, 1973; Dym et al., 2009; Ehmcke and Schlatt, 2006; Millar et al., 2000). In the adult marmoset testis, we clearly identified two major mutually exclusive populations of spermatogonia, SALL4$^+$PLZF$^+$LIN28$^+$ DPPA4$^+$DAZL$^+$, and C-KIT$^+$Ki67$^+$DAZL$^+$ (YDBIOI6681Figs. 1, 10, and Supplementary Fig. S1). Considering that Ki67 is an indicator for mitotic division, it is conceivable that SALL4$^+$PLZF$^+$LIN28$^+$DPPA4$^+$ DAZL$^+$ quiescent cells would represent A_{dark} spermatogonia while C-KIT$^+$Ki67$^+$DAZL$^+$ active cells would represent A_{pale} spermatogonia, as defined by differential BrdU (YDBIOI6681Ehmcke et al., 2005a, 2005bSimorangkir et al., 2009) or ^{3}H-thymidine incorporation (Clermont, 1969). This scenario fits with the finding of human spermatogonia that FGFR3$^+$UTF1$^+$ A_{dark} and C-KIT$^+$Ki67$^+$ A_{pale} spermatogonia can be detected in a mutually exclusive manner (von Kopylow et al., 2012). However, the relationship between the A_{dark}/A_{pale} classification and our molecular discrimination should be carefully considered because the only faithful biological basis of the A_{dark}/A_{pale} classification is due to their mitotic activity. Classical discrimination of spermatogonial subtypes by hematoxylin staining largely relies on researchers' proficiency, hence, is methodologically inadequate for accurate validation and data comparison among laboratories (Ehmcke and Schlatt, 2006). The conclusion can differ depending on the protocols, equipment, and even observers from each experiment. Of course, there is no doubt that this classical classification provided an informative guideline to advance developmental biology of the primate spermatogenesis. However, this strategy has become insufficient to fulfill the current diagnostic criteria in the late-breaking stem cell biology for specifying a particular cell type. We determined the spermatogonial subtypes with easily accessible but specific immunofluorescence by focusing on their mitotic activity. This brings out unequivocal, reliable identification of spermatogonia in the common marmoset, leading to further molecular dissections.

On the other hand, the molecular character of differentiated B spermatogonia remains to be determined. In the current study, we found that C-KIT$^+$ spermatogonia are comprised of Ki67$^+$ and Ki67$^-$ cell subpopulations (Fig. 1B and Supplementary Fig. S2A). Furthermore, a part of C-KIT$^+$ spermatogonia exhibits the nucleus-diffuse, punctate γH2AX staining, as seen in the pre-pachytene spermatocytes (Supplementary Fig. S2B). Given that γH2AX protein is predominantly enriched in spermatocytes (Fig. 4) and the nucleus-diffuse γH2AX protein is also present in mouse B spermatogonia (Hamer et al., 2003), C-KIT$^+$Ki67$^-$DAZL$^+$γH2AX$^+$ spermatogonia might represent marmoset B spermatogonia.

At the onset of spermatogenesis, it seems that gene expression undergoes the sequential processes as follows (Fig. 10). The early spermatocytes derived from spermatogonia can be recognized as DAZL$^+$γH2AX$^+$CLGN^{weak+} cells, in which the γH2AX protein is widely distributed in the whole nucleus in a punctate manner. At the pachytene stage, spermatocytes become DAZL$^+$γH2AX$^+$ CLGN$^+$VASA$^+$RanBPM$^+$SYCP1$^+$MARWI$^+$. In their nuclei, the γH2AX protein becomes confined to the XY body while SYCP1 protein localizes at the synaptonemal complexes. Then, round spermatids lose DAZL, γH2AX, and SYCP1 proteins but still express CLGN, VASA, RanBPM, and MARWI proteins. Finally, MARWI$^+$HAPRIN$^+$ elongating spermatids and spermatozoa appear. Thus, we describe the basic scheme of gene expression dynamics during marmoset spermatogenesis, but the information is still limited to a subset of genes. Nevertheless greater exploration of primate spermatogenesis is needed.

In addition to adult spermatogenesis, we also investigated gene expression dynamics in the sexually immature period before puberty. In the neonatal testis, gonocytes express SALL4 and C-KIT as well as DAZL and VASA proteins (Fig. 9) (Lin et al., 2012). During juvenile development, the gonocytes migrate to the basal membrane (McKinnell et al., 2013) where they form the SALL4$^+$ or C-KIT$^+$ spermatogonia. It is uncertain whether both types of spermatogonia are directly derived from the gonocytes. Considering gene expression in the adult spermatogonia, SALL4$^+$C-KIT$^+$DAZL$^+$VASA$^+$ gonocytes would turn to SALL4$^+$DAZL$^+$ spermatogonia while losing C-KIT and VASA expression. The SALL4$^+$DAZL$^+$ spermatogonia would subsequently give rise to C-KIT$^+$DAZL$^+$ spermatogonia.

On the other hand, some DAZL$^+$VASA$^+$ germ cells remain in the lumen of the juvenile seminiferous tubule (Fig. 5) (Lin et al., 2012). Previously, two types of germ cells could be observed in prepubertal marmoset testis; one in a central tubular position and the other at the basement membrane (Li et al., 2005). The identity of the centrally located germ cells, named pre-spermatogonia, had

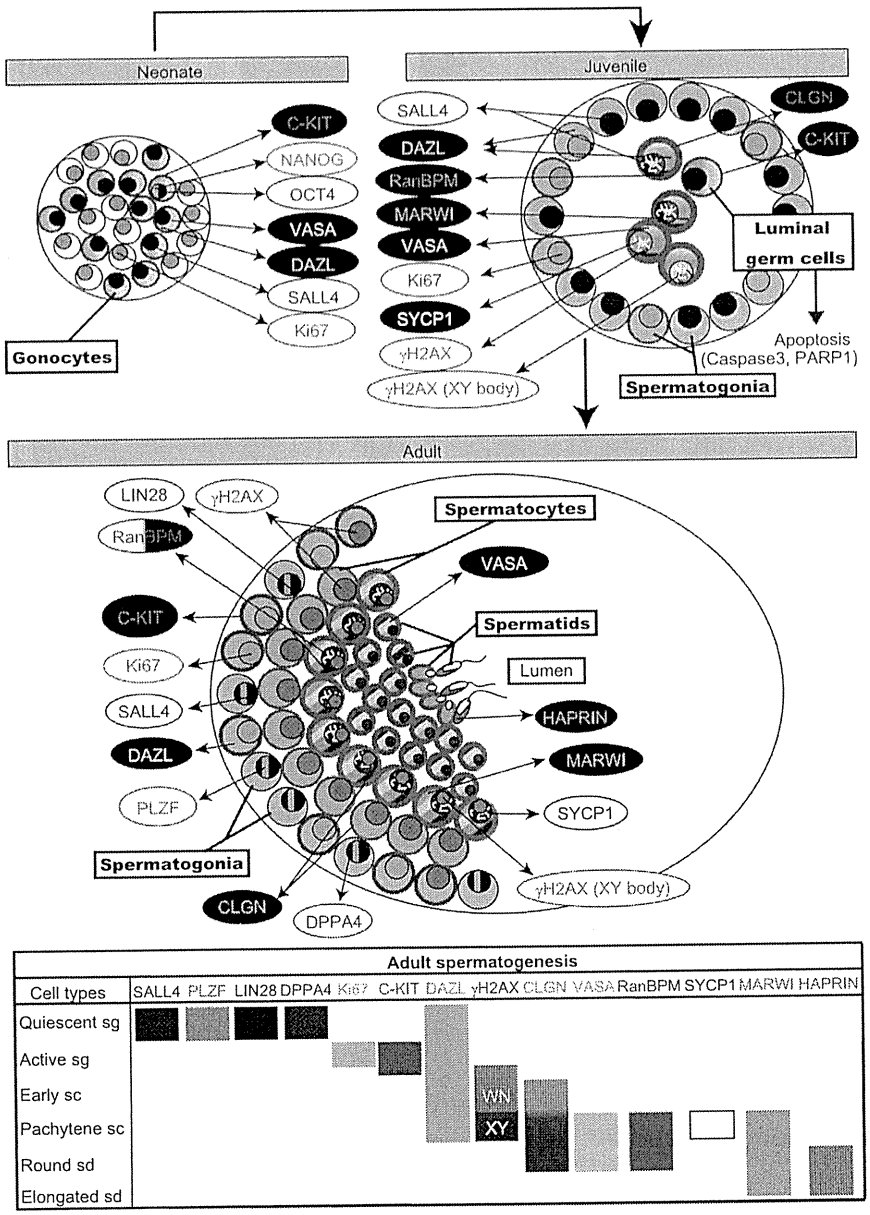

Fig. 10. A scheme of gene expression dynamics in the marmoset spermatogenesis. Schematic representation of spermatogenic development from neonate to adult in the common marmoset. In the seminiferous cords of neonatal testis, gonocytes express SALL4, C-KIT, DAZL, and VASA proteins. Pluripotency factors OCT4 and NANOG can be also observed in some of the gonocytes (Lin et al., 2012). Ki67 is present in non-germ cells, possibly Sertoli cell precursors. In the juvenile period, gonocytes relocated to the basement membrane turn to the member of the spermatogonial population. However, some gonocytes are left in the luminal region of seminiferous tubules. They lose the gonocyte gene expression and exhibit the spermatocyte-like expression, including DAZL, γH2AX, CLGN, VASA, RanBPM (cytoplasmic), SYCP1, MARWI proteins as well as an apoptosis marker (activated Caspase3, cleavage PARP1). In adult testis, SALL4$^+$PLZF$^+$LIN28$^+$DPPA4$^+$DAZL$^+$ quiescent spermatogonia (Quiescent sg) and C-KIT$^+$Ki67$^+$DAZL$^+$ active spermatogonia (Active sg) can be seen on the basement membrane. Upon differentiation, early spermatocytes (early sc) are recognized as DAZL$^+$γH2AX$^+$CLGN^{weak+} cells. At this stage, the distribution of γH2AX protein is in the whole nucleus (WN). Then, pachytene spermatocytes (pachytene sc) turn to be DAZL$^+$γH2AX$^+$CLGN$^+$VASA$^+$RanBPM$^+$SYCP1$^+$MARWI$^+$. The γH2AX protein is confined to the XY body (XY). Round spermatids (round sd) still express CLGN, VASA, RanBPM, and MARWI proteins. Finally, MARWI$^+$HAPRIN$^+$ elongating and elongated spermatids (elongated sd) and spermatozoa appear.

not been elucidated, but it turned out that these cells exhibited meiosis-associated gene expression. Nevertheless, the meiotic process seemed irregular, and the pre-spermatogonia result in apoptosis. In general, during development, germ cells should be recruited to the appropriate niches. If primordial germ cells are misdirected from the normal path, they undergo apoptosis (Tres et al., 2004). Likewise, migration failure to the basement membrane induces apoptosis in mouse gonocytes (YDBIOI6681Orth et al., 2000; Tres and Kierszenbaum, 2005). Taking this into account, we speculate that a part of the marmoset gonocytes might fail to migrate to the basement membrane and be eliminated by apoptosis through a meiosis-like process in the juvenile period. This scenario is also supported by cytoplasmic localization of RanBPM protein observed in pre-spermatogonia, which indicates the activation of an apoptotic pathway (Atabakhsh et al., 2009). However, we can still not exclude another possibility that the pre-spermatogonia might be abnormal spermatocytes derived from the start-up spermatogonia. In this assumption, the pre-spermatogonia (spermatocytes) might be located ectopically in the luminal region of the seminiferous tubules because of

immaturity of testicular niche and hormonal regulation (Li et al., 2005), which cannot support meiosis properly. In order to determine the origin of the pre-spermatogonia, further comprehensive, serial dissection of gene expression dynamics focusing on the neonatal-juvenile period is needed.

Following testicular development, juvenile spermatogonia start producing spermatocytes (YDBIOI6681Figs. 6 and 7), most of which are positive for activated Caspase3 (Fig. 8). Since the first wave of spermatogenesis mobilized after birth is accompanied by massive apoptosis of spermatocytes in rodents (Rodriguez et al., 1997), this could also occur in the common marmoset. On the other hand, unlike the pre-spermatogonia, cleavage PARP1 was not observed in the spermatocytes (Fig. 8). This could be explained by the different time course of apoptosis between pre-spermatogonia and spermatocytes. The pre-spermatogonia appeared earlier than the spermatocytes did during testicular development. Indeed, many activated caspase3- and cleavage PARP1-negative pre-spermatogonia existed in the less mature juvenile testis, in which the spermatocytes did not appear (Fig. 8). As the cleavage of PARP1 is implemented by the activated caspase3 (YDBIOI6681Agarwal et al., 2009; D'Amours et al., 2001; Said et al., 2004), the spermatocytes may become positive for cleavage PARP1 in later development.

In conclusion, we investigated molecular signatures of germ cells during postnatal testicular development in the common marmoset, which defined gene expression involved with developmental transitions. This also clarified, at least partly, the characteristics of primate germ cells, especially in the juvenile period. We expect that this fundamental ontogeny promotes better understanding of the primate germ cells and reproduction thereafter.

Acknowledgments

We thank Orie Hikabe, Kimie Ohta, Kazumichi M. Nishida, Miharu K. Kamatani, and Hirotaka James Okano for technical assistance, scientific discussions, and other support. This work was supported by Grants from the Ministry of Education, Culture, Sports, Science, and Technology of Japan (MEXT); the Ministry of Health, Labour and Welfare; the Japan Society for the Promotion of Science (JSPS); the National Institute of Biomedical Innovation; the Strategic Research Program for Brain Sciences and Leading Project for Realization of Regenerative Medicine, MEXT; the Project for Realization of Regenerative Medicine, MEXT; the Funding Program for World-Leading Innovative R&D in Science and Technology (FIRST); a Keio University Grant-in-Aid for the Encouragement of Young Medical Scientists; Leave a Nest Grant Life Technologies Japan Award; Interuniversity Bio-Backup Project for Basic Biology; and Otsuka Toshimi Foundation.

Appendix A. Supplementary materials

Supplementary data associated with this article can be found in the online version at http://dx.doi.org/10.1016/j.ydbio.2015.01.014.

References

Aeckerle, N., Eildermann, K., Drummer, C., Ehmcke, J., Schweyer, S., Lerchl, A., Bergmann, M., Kliesch, S., Gromoll, J., Schlatt, S., Behr, R., 2012. The pluripotency factor LIN28 in monkey and human testes: a marker for spermatogonial stem cells? Mol. Hum. Reprod. 18, 477–488.

Agarwal, A., Mahfouz, R.Z., Sharma, R.K., Sarkar, O., Mangrola, D., Mathur, P.P., 2009. Potential biological role of poly (ADP-ribose) polymerase (PARP) in male gametes. Reprod. Biol. Endocrinol. 7, 143.

Albert, S., Ehmcke, J., Wistuba, J., Eildermann, K., Behr, R., Schlatt, S., Gromoll, J., 2010. Germ cell dynamics in the testis of the postnatal common marmoset monkey (*Callithrix jacchus*). Reproduction 140, 733–742.

Atabakhsh, E., Bryce, D.M., Lefebvre, K.J., Schild-Poulter, C., 2009. RanBPM has proapoptotic activities that regulate cell death pathways in response to DNA damage. Mol. Cancer Res. 7, 1962–1972.

Chemes, H.E., 2001. Infancy is not a quiescent period of testicular development. Int. J. Androl. 24, 2–7.

Clermont, Y., 1963. The cycle of the seminiferous epithelium in man. Am. J. Anat. 112, 35–51.

Clermont, Y., 1966. Renewal of spermatogonia in man. Am. J. Anat. 118, 509–524.

Clermont, Y., 1969. Two classes of spermatogonial stem cells in the monkey (Cercopithecus aethiops). Am. J. Anat. 126, 57–71.

Clermont, Y., 1972. Kinetics of spermatogenesis in mammals: seminiferous epithelium cycle and spermatogonial renewal. Physiol. Rev. 52, 198–236.

Clermont, Y., Antar, M., 1973. Duration of the cycle of the seminiferous epithelium and the spermatogonial renewal in the monkey Macaca arctoides. Am. J. Anat. 136, 153–165.

Culty, M., 2009. Gonocytes, the forgotten cells of the germ cell lineage. Birth Defects Res. C Embryo Today 87, 1–26.

Culty, M., 2013. Gonocytes, from the fifties to the present: is there a reason to change the name? Biol. Reprod. 89, 46.

D'Amours, D., Sallmann, F.R., Dixit, V.M., Poirier, G.G., 2001. Gain-of-function of poly (ADP-ribose) polymerase-1 upon cleavage by apoptotic proteases: implications for apoptosis. J. Cell Sci. 114, 3771–3778.

de Vries, M., Vosters, S., Merkx, G., D'Hauwers, K., Wansink, D.G., Ramos, L., de Boer, P., 2012. Human male meiotic sex chromosome inactivation. PLoS One 7, e31485.

Deng, W., Lin, H., 2002. miwi, a murine homolog of piwi, encodes a cytoplasmic protein essential for spermatogenesis. Dev. Cell 2, 819–830.

Dreef, H.C., Van Esch, E., De Rijk, E.P., 2007. Spermatogenesis in the cynomolgus monkey (*Macaca fascicularis*): a practical guide for routine morphological staging. Toxicol. Pathol. 35, 395–404.

Dym, M., Kokkinaki, M., He, Z., 2009. Spermatogonial stem cells: mouse and human comparisons. Birth Defects Res. C Embryo Today 87, 27–34.

Ehmcke, J., Luetjens, C.M., Schlatt, S., 2005a. Clonal organization of proliferating spermatogonial stem cells in adult males of two species of non-human primates, *Macaca mulatta* and *Callithrix jacchus*. Biol. Reprod. 72, 293–300.

Ehmcke, J., Schlatt, S., 2006. A revised model for spermatogonial expansion in man: lessons from non-human primates. Reproduction 132, 673–680.

Ehmcke, J., Simorangkir, D.R., Schlatt, S., 2005b. Identification of the starting point for spermatogenesis and characterization of the testicular stem cell in adult male rhesus monkeys. Hum. Reprod. 20, 1185–1193.

Ehmcke, J., Wistuba, J., Schlatt, S., 2006. Spermatogonial stem cells: questions, models and perspectives. Hum. Reprod. Update 12, 275–282.

Eildermann, K., Aeckerle, N., Debowski, K., Godmann, M., Christiansen, H., Heistermann, M., Schweyer, S., Bergmann, M., Kliesch, S., Gromoll, J., Ehmcke, J., Schlatt, S., Behr, R., 2012. Developmental expression of the pluripotency factor sal-like protein 4 in the monkey, human and mouse testis: restriction to premeiotic germ cells. Cells Tissues Organs 196, 206–220.

Gassei, K., Orwig, K.E., 2013. SALL4 expression in gonocytes and spermatogonial clones of postnatal mouse testes. PLoS One 8, e53976.

Gerdes, J., Lemke, H., Baisch, H., Wacker, H.H., Schwab, U., Stein, H., 1984. Cell cycle analysis of a cell proliferation-associated human nuclear antigen defined by the monoclonal antibody Ki-67. J. Immunol. 133, 1710–1715.

Hamer, G., Roepers-Gajadien, H.L., van Duyn-Goedhart, A., Gademan, I.S., Kal, H.B., van Buul, P.P., de Rooij, D.G., 2003. DNA double-strand breaks and gamma-H2AX signaling in the testis. Biol. Reprod. 68, 628–634.

Haruyama, E., Suda, M., Ayukawa, Y., Kamura, K., Mizutamari, M., Ooshima, Y., Tanimoto, A., 2012. Testicular development in cynomolgus monkeys. Toxicol. Pathol. 40, 935–942.

Hermann, B.P., Sukhwani, M., Hansel, M.C., Orwig, K.E., 2010. Spermatogonial stem cells in higher primates: are there differences from those in rodents? Reproduction 139, 479–493.

Hermann, B.P., Sukhwani, M., Lin, C.C., Sheng, Y., Tomko, J., Rodriguez, M., Shuttleworth, J.J., McFarland, D., Hobbs, R.M., Pandolfi, P.P., Schatten, G.P., Orwig, K.E., 2007. Characterization, cryopreservation, and ablation of spermatogonial stem cells in adult rhesus macaques. Stem Cells 25, 2330–2338.

Hermann, B.P., Sukhwani, M., Simorangkir, D.R., Chu, T., Plant, T.M., Orwig, K.E., 2009. Molecular dissection of the male germ cell lineage identifies putative spermatogonial stem cells in rhesus macaques. Hum. Reprod. 24, 1704–1716.

Hermo, L., Pelletier, R.M., Cyr, D.G., Smith, C.E., 2010. Surfing the wave, cycle, life history, and genes/proteins expressed by testicular germ cells. Part 1: background to spermatogenesis, spermatogonia, and spermatocytes. Microsc. Res. Tech. 73, 241–278.

Hirano, T., Iwasaki, Y.W., Lin, Z.Y., Imamura, M., Seki, N.M., Sasaki, E., Saito, K., Okano, H., Siomi, M.C., Siomi, H., 2014. Small RNA profiling and characterization of piRNA clusters in the adult testes of the common marmoset, a model primate. RNA.

Hobbs, R.M., Fagoonee, S., Papa, A., Webster, K., Altruda, F., Nishinakamura, R., Chai, L., Pandolfi, P.P., 2012. Functional antagonism between Sall4 and Plzf defines germline progenitors. Cell Stem Cell 10, 284–298.

Imamura, M., Hikabe, O., Lin, Z.Y., Okano, H., 2014. Generation of germ cells in vitro in the era of induced pluripotent stem cells. Mol. Reprod. Dev. 81, 2–19.

Imamura, M., Miura, K., Iwabuchi, K., Ichisaka, T., Nakagawa, M., Lee, J., Kanatsu-Shinohara, M., Shinohara, T., Yamanaka, S., 2006. Transcriptional repression and DNA hypermethylation of a small set of ES cell marker genes in male germline stem cells. BMC Dev. Biol. 6, 34.

Imamura, M., Okuno, H., Tomioka, I., Kawamura, Y., Lin, Z.Y., Nakajima, R., Akamatsu, W., Okano, H.J., Matsuzaki, Y., Sasaki, E., Okano, H., 2012. Derivation of induced pluripotent stem cells by retroviral gene transduction in mammalian species. Methods Mol. Biol. 925, 21–48.
Jackson, M.R., Edmunds, J.G., 1984. Morphological assessment of testicular maturity in marmosets (*Callithrix jacchus*). Lab. Anim. 18, 173–178.
Kelnar, C.J., McKinnell, C., Walker, M., Morris, K.D., Wallace, W.H., Saunders, P.T., Fraser, H.M., Sharpe, R.M., 2002. Testicular changes during infantile 'quiescence' in the marmoset and their gonadotrophin dependence: a model for investigating susceptibility of the prepubertal human testis to cancer therapy? Hum. Reprod. 17, 1367–1378.
Kishi, N., Sato, K., Sasaki, E., Okano, H., 2014. Common marmoset as a new model animal for neuroscience research and genome editing technology. Dev. Growth Differ. 56, 53–62.
Kitamura, K., Nishimura, H., Nishimune, Y., Tanaka, H., 2005. Identification of human HAPRIN potentially involved in the acrosome reaction. J. Androl. 26, 511–518.
Kitamura, K., Tanaka, H., Nishimune, Y., 2003. Haprin, a novel haploid germ cell-specific RING finger protein involved in the acrosome reaction. J. Biol. Chem. 278, 44417–44423.
Kotaja, N., Sassone-Corsi, P., 2007. The chromatoid body: a germ-cell-specific RNA-processing centre. Nat. Rev. Mol. Cell Biol. 8, 85–90.
Kuramochi-Miyagawa, S., Kimura, T., Ijiri, T.W., Isobe, T., Asada, N., Fujita, Y., Ikawa, M., Iwai, N., Okabe, M., Deng, W., Lin, H., Matsuda, Y., Nakano, T., 2004. Mili, a mammalian member of piwi family gene, is essential for spermatogenesis. Development 131, 839–849.
Li, L.H., Donald, J.M., Golub, M.S., 2005. Review on testicular development, structure, function, and regulation in common marmoset. Birth Defects Res. B Dev. Reprod. Toxicol. 74, 450–469.
Lin, Z.Y., Imamura, M., Sano, C., Nakajima, R., Suzuki, T., Yamadera, R., Takehara, Y., Okano, H.J., Sasaki, E., Okano, H., 2012. Molecular signatures to define spermatogenic cells in common marmoset (*Callithrix jacchus*). Reproduction 143, 597–609.
Mahadevaiah, S.K., Turner, J.M., Baudat, F., Rogakou, E.P., de Boer, P., Blanco-Rodriguez, J., Jasin, M., Keeney, S., Bonner, W.M., Burgoyne, P.S., 2001. Recombinational DNA double-strand breaks in mice precede synapsis. Nat. Genet. 27, 271–276.
Maldonado-Saldivia, J., van den Bergen, J., Krouskos, M., Gilchrist, M., Lee, C., Li, R., Sinclair, A.H., Surani, M.A., Western, P.S., 2007. Dppa2 and Dppa4 are closely linked SAP motif genes restricted to pluripotent cells and the germ line. Stem Cells 25, 19–28.
Mansfield, K., 2003. Marmoset models commonly used in biomedical research. Comp. Med. 53, 383–392.
McKinnell, C., Mitchell, R.T., Morris, K., Anderson, R.A., Kelnar, C.J., Wallace, W.H., Sharpe, R.M., 2013. Perinatal germ cell development and differentiation in the male marmoset (*Callithrix jacchus*): similarities with the human and differences from the rat. Hum. Reprod. 28, 886–896.
Millar, M.R., Sharpe, R.M., Weinbauer, G.F., Fraser, H.M., Saunders, P.T., 2000. Marmoset spermatogenesis: organizational similarities to the human. Int. J. Androl. 23, 266–277.
Mitchell, R.T., Cowan, G., Morris, K.D., Anderson, R.A., Fraser, H.M., McKenzie, K.J., Wallace, W.H., Kelnar, C.J., Saunders, P.T., Sharpe, R.M., 2008. Germ cell differentiation in the marmoset (*Callithrix jacchus*) during fetal and neonatal life closely parallels that in the human. Hum. Reprod. 23, 2755–2765.
Monesi, V., 1965. Synthetic activities during spermatogenesis in the mouse RNA and protein. Exp. Cell Res. 39, 197–224.
Okano, H., Hikishima, K., Iriki, A., Sasaki, E., 2012. The common marmoset as a novel animal model system for biomedical and neuroscience research applications. Semin Fetal Neonatal Med. 17, 336–340.
Orth, J.M., Jester, W.F., Li, L.H., Laslett, A.L., 2000. Gonocyte-Sertoli cell interactions during development of the neonatal rodent testis. Curr. Top. Dev. Biol. 50, 103–124.
Page, S.L., Hawley, R.S., 2004. The genetics and molecular biology of the synaptonemal complex. Annu. Rev. Cell Dev. Biol. 20, 525–558.
Pousette, A., Leijonhufvud, P., Arver, S., Kvist, U., Pelttari, J., Hoog, C., 1997. Presence of synaptonemal complex protein 1 transversal filament-like protein in human primary spermatocytes. Hum. Reprod. 12, 2414–2417.
Puverel, S., Barrick, C., Dolci, S., Coppola, V., Tessarollo, L., 2011. RanBPM is essential for mouse spermatogenesis and oogenesis. Development 138, 2511–2521.
Rey, R.A., Campo, S.M., Bedecarras, P., Nagle, C.A., Chemes, H.E., 1993. Is infancy a quiescent period of testicular development? Histological, morphometric, and functional study of the seminiferous tubules of the cebus monkey from birth to the end of puberty. J. Clin. Endocrinol. Metab. 76, 1325–1331.
Rodriguez, I., Ody, C., Araki, K., Garcia, I., Vassalli, P., 1997. An early and massive wave of germinal cell apoptosis is required for the development of functional spermatogenesis. EMBO J. 16, 2262–2270.
Ruggiu, M., Saunders, P.T., Cooke, H.J., 2000. Dynamic subcellular distribution of the DAZL protein is confined to primate male germ cells. J. Androl. 21, 470–477.
Said, T.M., Paasch, U., Glander, H.J., Agarwal, A., 2004. Role of caspases in male infertility. Hum. Reprod. Update 10, 39–51.
Sasaki, E., Suemizu, H., Shimada, A., Hanazawa, K., Oiwa, R., Kamioka, M., Tomioka, I., Sotomaru, Y., Hirakawa, R., Eto, T., Shiozawa, S., Maeda, T., Ito, M., Ito, R., Kito, C., Yagihashi, C., Kawai, K., Miyoshi, H., Tanioka, Y., Tamaoki, N., Habu, S., Okano, H., Nomura, T., 2009. Generation of transgenic non-human primates with germline transmission. Nature 459, 523–527.
Sasaki, T., Shiohama, A., Minoshima, S., Shimizu, N., 2003. Identification of eight members of the Argonaute family in the human genome. Genomics 82, 323–330.
Saunders, P.T., Gaughan, J., Saxty, B.A., Kerr, L.E., Millar, M.R., 1996. Expression of protamine P2 in the testis of the common marmoset and man visualized using non-radioactive in-situ hybridization. Int. J. Androl. 19, 212–219.
Schlatt, S., Ehmcke, J., 2014. Regulation of spermatogenesis: an evolutionary biologist's perspective. Semin. Cell Dev. Biol. 29C, 2–16.
Sharpe, R.M., Fraser, H.M., Brougham, M.F., McKinnell, C., Morris, K.D., Kelnar, C.J., Wallace, W.H., Walker, M., 2003. Role of the neonatal period of pituitary-testicular activity in germ cell proliferation and differentiation in the primate testis. Hum. Reprod. 18, 2110–2117.
Shibata, N., Tsunekawa, N., Okamoto-Ito, S., Akasu, R., Tokumasu, A., Noce, T., 2004. Mouse RanBPM is a partner gene to a germline specific RNA helicase, mouse vasa homolog protein. Mol. Reprod. Dev. 67, 1–7.
Simorangkir, D.R., Marshall, G.R., Plant, T.M., 2009. A re-examination of proliferation and differentiation of type A spermatogonia in the adult rhesus monkey (*Macaca mulatta*). Hum. Reprod. 24, 1596–1604.
Siomi, M.C., Sato, K., Pezic, D., Aravin, A.A., 2011. PIWI-interacting small RNAs: the vanguard of genome defence. Nat. Rev. Mol. Cell Biol. 12, 246–258.
Takahashi, T., Hanazawa, K., Inoue, T., Sato, K., Sedohara, A., Okahara, J., Suemizu, H., Yagihashi, C., Yamamoto, M., Eto, T., Konno, Y., Okano, H., Suematsu, M., Sasaki, E., 2014. Birth of healthy offspring following icsi in in vitro-matured common marmoset (*Callithrix jacchus*) oocytes. PLoS One 9, e95560.
Tomioka, I., Takahashi, T., Shimada, A., Yoshioka, K., Sasaki, E., 2012. Birth of common marmoset (Callithrix jacchus) offspring derived from in vitro-matured oocytes in chemically defined medium. Theriogenology 78, 1487–1493.
Tres, L.L., Kierszenbaum, A.L., 2005. The ADAM-integrin-tetraspanin complex in fetal and postnatal testicular cords. Birth Defects Res. C Embryo Today 75, 130–141.
Tres, L.L., Rosselot, C., Kierszenbaum, A.L., 2004. Primordial germ cells: what does it take to be alive? Mol. Reprod. Dev. 68, 1–4.
von Kopylow, K., Staege, H., Schulze, W., Will, H., Kirchhoff, C., 2012. Fibroblast growth factor receptor 3 is highly expressed in rarely dividing human type A spermatogonia. Histochem. Cell Biol. 138, 759–772.
von Schonfeldt, V., Krishnamurthy, H., Foppiani, L., Schlatt, S., 1999. Magnetic cell sorting is a fast and effective method of enriching viable spermatogonia from Djungarian hamster, mouse, and marmoset monkey testes. Biol. Reprod. 61, 582–589.
Western, P.S., van den Bergen, J.A., Miles, D.C., Sinclair, A.H., 2010. Male fetal germ cell differentiation involves complex repression of the regulatory network controlling pluripotency. FASEB J. 24, 3026–3035.
Wistuba, J., Schrod, A., Greve, B., Hodges, J.K., Aslam, H., Weinbauer, G.F., Luetjens, C.M., 2003. Organization of seminiferous epithelium in primates: relationship to spermatogenic efficiency, phylogeny, and mating system. Biol. Reprod. 69, 582–591.
Yamauchi, K., Hasegawa, K., Chuma, S., Nakatsuji, N., Suemori, H., 2009. In vitro germ cell differentiation from cynomolgus monkey embryonic stem cells. PLoS One 4, e5338.
Yoshinaga, K., Tanii, I., Toshimori, K., 1999. Molecular chaperone calmegin localization to the endoplasmic reticulum of meiotic and post-meiotic germ cells in the mouse testis. Arch. Histol. Cytol. 62, 283–293.

Microscopy Advance Access published December 18, 2014

MICROSCOPY

Microscopy, 2014, 1–11
doi: 10.1093/jmicro/dfu103

Review

Connectomics: comprehensive approaches for whole-brain mapping

Shinsuke Shibata[1,*], Yuji Komaki[1,2], Fumiko Seki[1], Michiko O. Inouye[1], Toshihiro Nagai[3], and Hideyuki Okano[1,4,*]

[1]Department of Physiology, Keio University School of Medicine, 35 Shinanomachi, Shinjuku-ku, Tokyo 160-8582, Japan, [2]Central Institute for Experimental Animals, Tonomachi 3-25-12, Kawasaki-ku, Kawasaki, Kanagawa 210-0821, Japan, [3]Electron Microscope Laboratory, Keio University School of Medicine, 35 Shinanomachi, Shinjuku-ku, Tokyo 160-8582, Japan, and [4]Laboratory for Marmoset Neural Architecture, RIKEN Brain Science Institute, 2-1 Hirosawa, Wako, Saitama 351-0198, Japan

*To whom correspondence should be addressed. E-mail: shibata@2001.jukuin.keio.ac.jp; hidokano@a2.keio.jp

Received 15 October 2014; Accepted 16 November 2014

Abstract

The aim of connectomics analysis is to understand whole-brain neural connections. This is accomplished using new biotechnologies. Here, we provide an overview of the recent progress in connectomics analysis. The entire neural network of an organism was revealed for the first time in the nematode. *Caenorhabditis elegans* (*C. elegans*) have an advantage of their limited number of neurons and their transparency, allowing the neural network to be visualized using light and electron microscopes (EMs). It is practically impossible to adopt the same approach for mammals because of the large number of neural cells and the opacity of the central nervous system. A variety of new technologies are being developed to perform computer-assisted high-throughput image acquisition and analysis to obtain whole-brain maps for higher species, including mammals. Diffusion tensor magnetic resonance imaging and tractography and three-dimensional imaging with the EM are examples of novel approaches to connectomics. These new technologies will soon be applied not only to *Drosophila*, *C. elegans* and rodent research, but also to comprehensive connectomics analysis in a wide range of species including humans and primates. In the near future, results from connectomics analysis will reveal the neural circuitry of the whole brain and enhance our understanding of the human mind and neuropsychiatric diseases.

Key words: connectomics, connectome, brain mapping, magnetic resonance imaging, electron microscope, serial EM

Introduction

Large grants for brain connectomics analyses were recently launched all over the world, including Europe, the United States and Japan. In 2013, the Human Brain Project started in Europe. This aims to provide researchers worldwide with tools to understand how the human brain works by using unique simulation-based approaches. At the same time, President Obama in the United States emphasized the

importance of brain mapping in the State of the Union Address as follows: 'Now, if we want to make the best products, we also have to invest in the best ideas. Every dollar we invested to map the human genome returned $140 to our economy – every dollar. Today, our scientists are mapping the human brain to unlock the answers to Alzheimer's. They're developing drugs to regenerate damaged organs; devising new material to make batteries 10 times more powerful. Now is not the time to gut these job-creating investments in science and innovation. Now is the time to reach a level of research and development not seen since the height of the Space Race. We need to make those investments.' (http://www.whitehouse.gov/state-of-the-union-2013) (last accessed date 3 December 2014). This statement led to the creation of the NIH-funded BRAIN (Brain Research Through Advancing Innovative Neurotechnologies) Initiative grant, which began in the United States in 2013. In Europe, the Human Brain Project, which is one of two Future and Emerging Technologies Flagship Initiatives, was launched by the European Commission in 2013 (http://cordis.europa.eu/fp7/ict/programme/fet/flagship/) (last accessed date 3 December 2014). In 2014, a brain mapping project called Brain/MINDS (Brain Mapping by Integrated Neurotechnologies for Disease Studies) officially started in Japan, aimed at understanding the mechanisms of the mind (http://brainminds.jp) (last accessed date 3 December 2014) by taking advantage of the non-human primate brain, especially the common marmoset (*Callithrix jacchus*) brain [1,2]. Comprehensive mapping studies of the non-human primate brain are essential for understanding the human brain and for developing knowledge-based strategies for the diagnosis and treatment of psychiatric and neurological disorders. The common marmoset is a small New World non-human primate that is extensively used for this purpose in biomedical research. Understanding the mechanisms of the human mind by revealing the connectomics in the brain is one of the biggest challenges of the century in the science community all over the world.

As President Obama suggested in his 2013 State of the Union Address, the current status of the connectomics project echoes the history of the human genome project (HGP) several decades ago. The HGP was an international collaborative research project to determine the sequence of the whole human genome and map all the genes under the international partnership including the United States, Europe, Japan and China. The genome project was initially proposed by the United States government in the mid-1980s, officially started around 1990, and was completed in 2003. Now, we are at the beginning of the international connectomics project to determine the neural wiring diagram of the whole human brain and map all of the functional relations of the brain through collaborations in and between Europe, the United States and Japan.

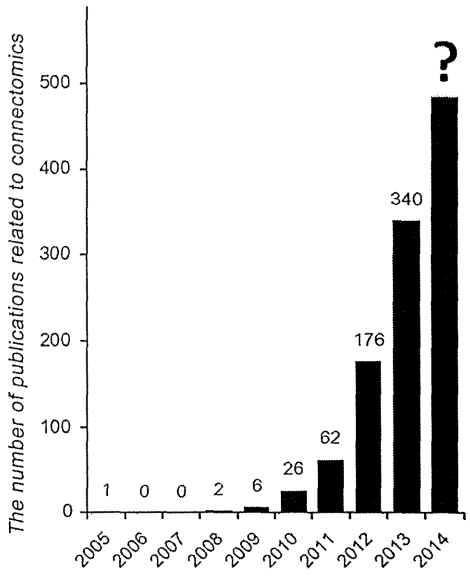

Fig. 1. The number of connectomics-related publications. According to the PubMed database, the number of publications related to connectomics analysis is increasing year by year. Papers with the keyword 'connectome' or 'connectomics' were counted.

What does connectomics stand for?

The word connectomics is relatively new and consists of two parts: one denotes the whole connection of the neural circuit (connect-) and the other refers to comprehensive analysis (-omics), similar to proteomics or to genomics. Recently, connectomics analysis has been in the spotlight as one of the new fields of research in neuroscience because it can provide structural bases for diverse functions of the human brain. As proof of the attention it has gained, an increasing number of papers have been published on connectomics over the last several years (Fig. 1). The number of publications related to connectomics was determined from a keyword search containing the words 'connectome' or 'connectomics' in the PubMed database (http://www.ncbi.nlm.nih.gov/pubmed) (last accessed date 3 December 2014). The meaning of the word 'connectomics' was explained by Prof. Jeff W. Lichtman at Harvard University as 'a branch of biotechnology concerned with applying the techniques of computer-assisted image acquisition and analysis to the structural mapping of sets of neural circuits or to the complete nervous system of selected organisms using high-speed methods, with organizing the results in databases, and with applications of the data' (iBiology by Jeff W. Lichtman, Part 1: connectomics: seeking neural circuit motifs).

The overall goal of connectomics analysis is to understand the whole neural circuit in the human brain, and this is accomplished using new biotechnologies. Thus, the progress of connectomics analysis requires not only active biological investigations but also technological advancements including the development of novel microscopes, new devices and drastic improvements in the computer programs available for analysis. In fact, many novel biotechnologies were invented especially for connectomics, including the multiple-beam scanning electron microscope (SEM) and automatic tape-collecting ultramicrotome (ATUM) and its software [3,4].

Connectomics and genomics

Connectomics describes the new field of research that focuses on the comprehensive analysis of neural connections. Connectomics may appear to be a subcategory within the field of neuroscience; however, connectomics and neuroscience are independent concepts that have their own independent territories. Classical methodologies for morphological experiments in cellular and anatomical neuroscience concern normal and abnormal functions of one or some neurons, but the target of connectomics is the whole network that exists among large numbers of neurons, beyond the function of the single neuron. The desinence of the word connectomics (i.e. -omics) is the same as that of the word genomics, and the relation between connectomics and neuroscience is quite similar to that between genomics and genetics. Genetics focuses on a specific mutation, abnormality or function of one or some genes, whereas genomics focuses on whole-genome function based on the integration of all genes and is beyond the function of a single gene. Based on the many findings in the field of genetics and reports on the functions of genes, genomics achieved great progress supported by large genome-project grants in the 1990s. After the completion of whole-genome sequencing of many species around the year 2000 [5,6], new approaches for genomics emerged, including comparative genomics. This is currently referred to as the post-genome era. One of the most important factors responsible for breakthroughs in the fields of genetics and genomics was the invention of DNA sequencers. The progress of genetics was supported by the development of the gel and capillary sequencers, and that of genomics was supported by the development of a variety of next-generation sequencers that incorporated various new concepts.

Progress in the field of neuroscience was supported by the invention of light microscopy (LM) in the era of Santiago Ramón y Cajal. Cajal is well-known for his artistic drawings of the neural network that were made using LM, and he was awarded the Nobel Prize in Physiology or Medicine in 1906 with Camillo Golgi, who is the developer of the Golgi stain [7]. Just like the next-generation sequencers for genomics, new machines and procedures that are currently beyond our imagination will help to progress the study of connectomics [3]. As mentioned above, big projects for connectomics supported by governments recently started all over the world, and we are hopeful for progress in understanding the human mind via revealing the whole neural wiring diagram in the near future.

History of recent approaches to connectomics

In the mid-1980s, the first full connectomics analysis was completed for the nematode, *Caenorhabditis elegans* (*C. elegans*), for which the neural diagram was constructed manually [8]. Micrographs of serially sectioned samples of hermaphroditic *C. elegans* were taken using electron microscopy (EM), and their reconstruction was performed almost entirely by hand. This full *C. elegans* connectomics analysis was preceded by a series of studies in the 1970s that used manual reconstruction of electron micrographs to visualize the neural wiring within various regions of the *C. elegans* nervous system [8–12]. Due to the limited number of neurons and their transparent body, *C. elegans* proved a favorable model for this manual technique of investigating every synaptic connection among all neurons. However, full connectomics was achieved only as a result of a massive amount of effort and time. It took more than a decade for White *et al.* to completely map the whole nematode nervous system of around 300 neurons. The same procedure would be expected to take about 2.5 million years for the mouse brain (~75 million neurons) and about 33 million years for the human brain (~100 billion neurons), highlighting a need for new technologies to map the human brain in a shorter period of time. The current approach to connectomics involves the use of tracers and transgene methods, and combining them with magnetic resonance imaging (MRI) and EM technologies, to make human connectomics more plausible.

One recent innovation developed for the purpose of connectomics analysis is the expression of multiple spectral and photophysical protein variants (XFPs) such as cyan, green, orange, red and yellow fluorescent proteins on a single transgene, resulting in differential color coding of individual neurons in over 100 colors, termed the Brainbow approach [13]. Its mechanism is based on the *Cre/loxP* recombination system. For example, in the Brainbow-1.0 strategy, canonical and mutant forms of *lox* sites are inserted at the ends of different XFPs (Fig. 2) [13]. Because *Cre* recombinase promotes recombination only between identical *lox* sites, inclusion/exclusion of the open reading frames (ORFs) of

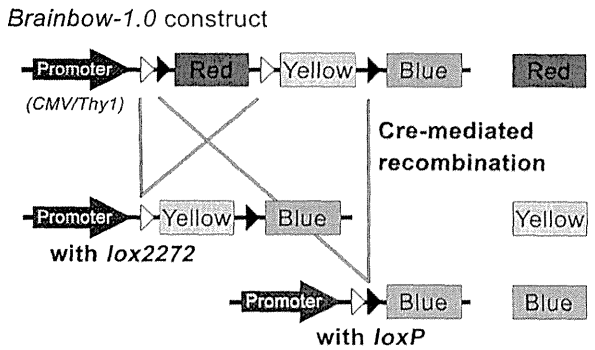

Fig. 2. The basic construct of Brainbow-1.0. A simplified version of the Brainbow-1.0 construct is illustrated, based on the original report [13].

multiple XFPs takes place in a mutually exclusive fashion. This drives stochastic expression of XFPs at varying degrees and combinations in individual neural cells. In Brainbow-2.1, two ORFs encoding different spectral variants of XFPs are placed in an opposite direction and flanked with *lox* sites, which promote both inversion and excision of this DNA cassette by the activity of *Cre* recombinase. When two of these invertible DNA cassettes were placed in tandem, three independent inversions can take place. This leads to a number of possible outcomes (larger than Brainbow-1.0) in XFP expression, all of which have equal probabilities.

The Brainbow technique can generate a broad color spectrum of over 100 different hues to label neurons. This combinatorial XFP expression allows for differential labeling of individual neurons and, in contrast to earlier fluorescence methods that made use of only two or three XFPs, the large size of the color palette drastically minimizes the likelihood of identical XFP expression in two adjacent neurons [14–17]. The Brainbow technique thus presents a novel way in which the precise projection of every neuron in the central and peripheral nervous system of the transgenic mouse can be visualized. Additionally, Brainbow technology possesses a remarkable versatility. In addition to differentiating distinct neurons, it allows researchers to distinguish mouse blastomere clones from one another in a recent study on blastomere allocation at the mouse embryo cleavage state [18]. The Brainbow technique also enables researchers to trace the lineage of neural progenitor cells [19]. Moreover, in addition to analyses of the mouse nervous system, Brainbow transgenes were recently used to draw neural wiring diagrams of the sensory nervous system of the zebrafish [20] and *Drosophila* [21,22].

Although the Brainbow technique allows multicolor visualization of individual neural connections, it presents a few limitations. For instance, a spectrum of 100 colors is sufficiently diverse in comparison to earlier fluorescence methods, but to view full regions of the nervous system, more colors must be produced to make up for the multiplicity of types of

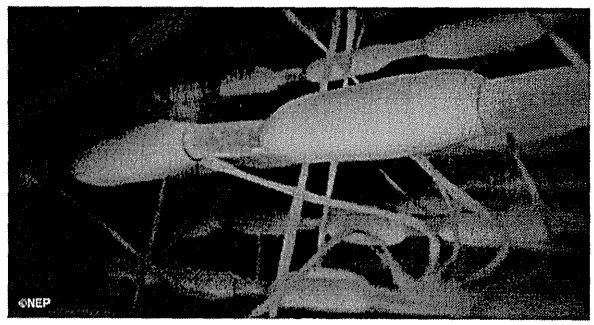

Fig. 3. An illustration of a myelinated fiber tract. DTI reflects water molecule anisotropy, which is mainly restricted by myelinated neural structures in the white matter. This is the computer graphic illustration which describes that the myelin structure from oligodendrocyte (green) wraps the neural fibers (ivory) and was kindly provided by NHK Enterprises, Inc.

neuronal cells being observed at once. In addition, a limitation concerning the low resolution of fluorescence images emerges when observing more complex neural wiring systems with LM, and this requires thinner sections to be obtained [23].

Macroscale, mesoscale and microscale connectomics

There are a lot of approaches to studying neural connectomics, and the approaches are on varying scales. MRI is a representative macroscale connectomics analysis technique that is used to detect the whole-brain wiring diagram. EM is a microscale connectomics analysis technique used to elucidate the microscopic neural connections at the synapse level. The LM approach, including the Brainbow technique, is categorized as mesoscale connectomics and aims to link the results from macroscale and microscale connectomics. In the following section, we describe and compare the main features of each approach.

Macroscale connectomics with MRI

One of the aims of connectomics is to map brain connectivity at the macro level and to unveil system-level connections. Non-invasive MRI is often chosen for macroscale connectome analysis. There are several advantages to using MRI, including the ability to perform *in vivo* longitudinal experiments, perform experiments across species, from mice to human beings and obtain and analyze data from the whole brain.

There were attempts to map structural connections with MRI by examining the presence of anatomical connections using cortical thickness measurements across the regions [24]. Diffusion MRI provides information about structural connectivity patterns by visualizing the spatial orientation

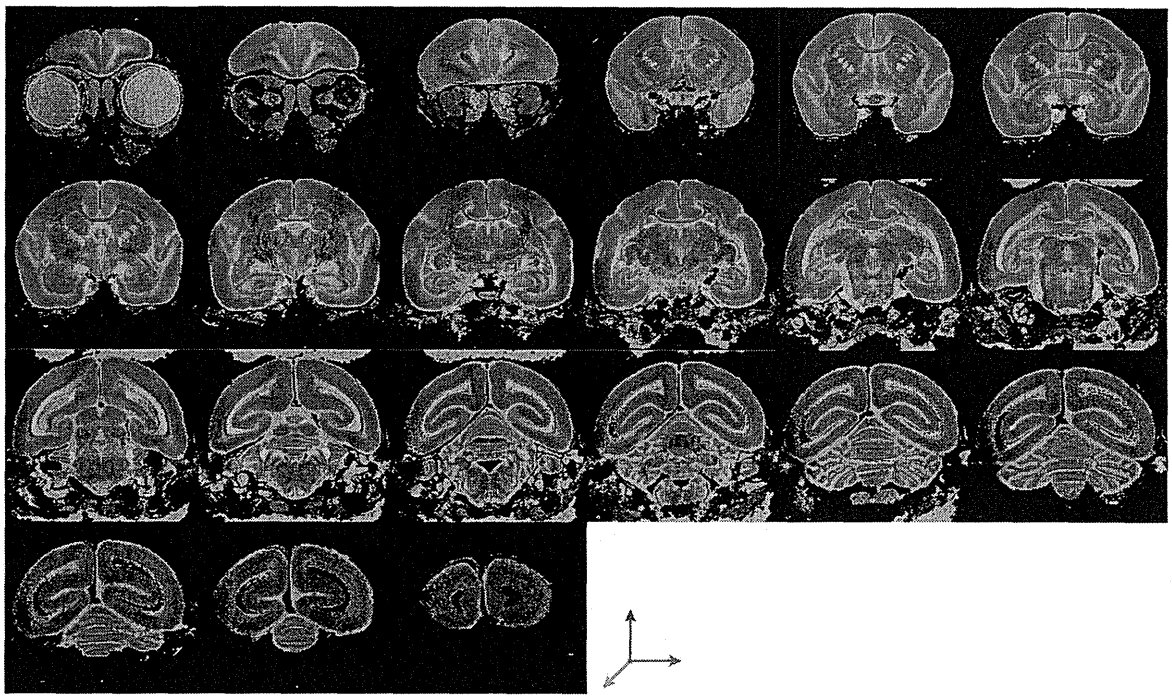

Fig. 4. Images from MRI connectomics analysis. Representative high-resolution DTI (120 μm isotropic) of the common marmoset brain overlaid with anatomical MRI. The color-coded map obtained from DTI shows white-matter structures identified through analysis of water molecule anisotropy. Colors indicate the fiber direction: green, antero-posterior; red, medio-lateral and blue, cranio-caudal.

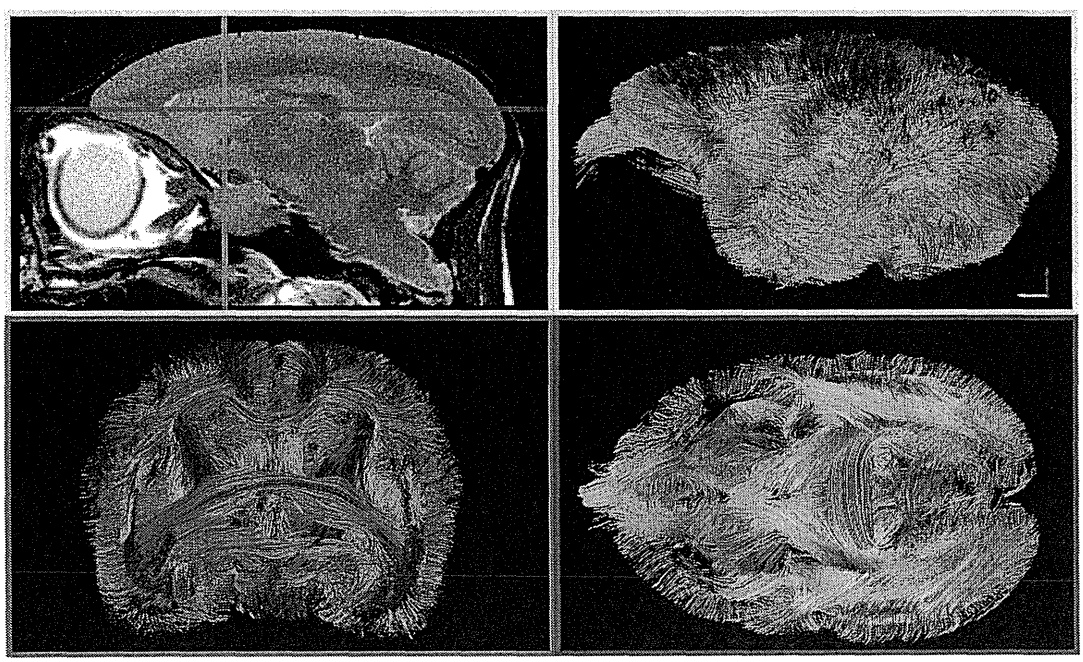

Fig. 5. The macroscale fiber connections of the whole brain identified using tractography. Tractography using DTI data can be used to identify fiber bundles in the common marmoset brain at the macroscale. Upper-left: Sagittal plane anatomical image. Upper-right: Lateral view of all fiber tracts, created using whole-brain tractography. Lower left: Fiber tracts from coronal section of the anatomical image (cyan) created using tractography. Lower right: Fiber tracts from axial section of the anatomical image (magenta) created using tractography. Colors indicate the fiber direction: green, antero-posterior; red, medio-lateral and blue, cranio-caudal.

of white-matter fiber tracts (Fig. 3) and is another approach used to map connectivity [25,26]. The most frequently used techniques are diffusion tensor imaging (DTI) (Fig. 4) and diffusion tensor tractography (Fig. 5) [27–29]. These techniques allow localization and study of the circuitries formed by major fiber tracts. Although analysis of crossing fibers presented a hurdle due to difficulties resolving multiple fiber bundle orientations inside imaging voxels [30], advanced techniques such as high angular resolution diffusion imaging (HARDI) and diffusion spectrum imaging (DSI) overcame this problem and allowed more precise evaluation of crossing fibers [31–34].

The organization of structural connectivity can be further studied by application to network analysis [26]. Analysis of diffusion MRI data with graph and network theory can provide further information about network characteristics, such as centrality and efficiency at the whole-brain level, to reveal brain neuronal communication and architectures [35]. The resulting network architectures contain rich but complex information. Circular visualization (referred to as connectograms) was developed to retrieve information from these analyses in an effective manner [36]. The comprehensive circle map allows visual classification of connective relations and makes it possible to detect abnormalities when applied to clinical data and animal models of disease [37]. The reliability of connectogram visualization of multidimensional information obtained from MRI can be increased by combining it with anatomical tract tracing. Cross validation of macroscale MRI analysis with an accurate histological analysis should be performed in the same experimental samples. A non-human primate, for example, a common marmoset, is a promising experimental resource for cross validation.

Microscale connectomics with EM, comparing to the macro and mesoscale

EM is used to observe ultrastructure in various applications, from the diagnosis of human biopsy samples to the histological observation of many kinds of tissues and their microstructure and organelles, including the synapse, cilia, mitochondria and myelin structure. The accelerated electrons enable structure to be visualized at the subcellular level. EM has a much higher resolution than LM due to the shorter wavelength of the electron compared with that of visible light. Although diffusion MRI analysis with an extremely high resolution was recently achieved [38], the resolution of MRI is still lower than that of LM and EM. For achieving the multiscale brain mapping, we have to take advantage of these three major technologies (LM, MRI and EM). The characteristics of each technology for connectomics analyses are summarized in Table 1.

Both MRI and EM analyses require highly skilled staff and expensive machines, but this is not the case for LM. If there is a support from skilled staff, MRI can easily image a whole brain, whether small (e.g. a mouse or rat brain) or large (e.g. a human or primate brain). EM imaging also requires skilled staff, and it is much more difficult to carry out whole-brain mapping, especially for a large brain like that of a human.

MRI is usually used for live imaging (Fig. 5) and is also used on the post-mortem brain to obtain high-resolution images (Fig. 4). LM can be used to image live and dead (fixed) samples and is generally used with fluorescence time-lapse imaging for live imaging and with multicolor immunostaining of fixed samples. Because of the low penetration of electrons to water, air and other substances, observation with EM generally requires a vacuum and ultrathin sectioning of the samples along with hard fixation. Live animal imaging with EM can be performed only with creative ingenuity, including the use of high vacuum-resistant creatures [39], vacuum-resistant surface modifications designated as nano-suit [40] or the use of special EM named atmospheric scanning electron microscope (ASEM), which detects dynamic phenomena in liquid or gas [41–43].

Microscale connectomics with serial EM

Serial EM is a great technology that utilizes the EM to obtain serial images from continuous sections. There is a long history for this technology pioneered by John K. Stevens, Kristen M. Harris and their colleagues from the early 1980s [44–47]. They developed a serial reconstruction system for collecting, photographing and analyzing the

Table 1. The three major technologies used for connectomics analysis

	Light/fluorescence microscopy	Magnetic resonance imaging	Electron microscopy
Imaging performed using	Light (fluorescence)	Magnetic resonance	Electron
Resolution	High	Low	Extremely high
Skill level required for imaging	Low	High	High
Expense	Moderate	High	High
Whole-brain imaging	Difficult	Easy	Very difficult
Live imaging	Easy	Easy	Difficult

continuous EM sections from the synapses and dendrites. Their effort makes it possible to observe the subcellular structure with extremely high resolution; much higher than can be obtained with LM or MRI. In addition, this EM-based approach enables quantitative three-dimensional evaluation of the precise location of synapses, vesicles, buttons, mitochondria, endoplasmic reticulum, ribosomes, cilia, myelin and other organelles in a micro-domain of the brain [48–50]. Serial EM has been widely applied to many projects to analyze the microstructure of cells and tissues in three dimensions with high resolution. An important characteristic of serial EM is that the serial image acquisition is carried out not only by a transmission electron microscope (TEM), but also by SEM. For general TEM observation in biology, the culture cells and tissues are fixed, dehydrated, embedded into plastic and ultrathin sectioned. In contrast, SEM analysis focuses on detecting the detailed surface information of the specimen through the critical point drying. The progress of SEM technology means that it is now possible to obtain high-resolution images with adequate contrast from the sectioned surface of biological samples. Primary challenges for the serial EM were carried out by using TEM; however, a new hybrid technique of SEM and TEM was recently developed [51]. The introduction of automated transmission-mode scanning electron microscopy (tSEM) for large volume reconstruction was reported. In addition, another group utilized TEM camera array (TEMCA) system, which is the combination of commercially available TEM and a large scintillator with four high-speed charge-coupled device (CCD) cameras for acquisition of large field view of serially sectioned EM samples efficiently [50].

As for the SEM-based techniques, there are two independent procedures used to obtain serial EM images of the surface from the resin-embedded tissue. One, designated as ATUM, is to collect all serial ultrathin sections on tape or glass, and the other is to carry out sectioning in a vacuum chamber for continuous observation on the block surface. There are three major SEM-based approaches for serial EM: the ATUM system with SEM (ATUM-SEM), the serial block-face SEM (SBF-SEM) and the focused ion beam-SEM (FIB-SEM). The characteristics of these approaches are summarized in Table 2. ATUM-SEM is a new procedure for serial EM that was developed by Prof. Jeff W. Lichtman and his group [4,52]. The block of the brain prepared for EM is embedded in plastic and sectioned to around 30 nm thickness, and the sections are automatically collected on a continuous plastic flexible tape using a conveyor-belt device called ATUM (Fig. 6). The ATUM device can generate a series (as many as several tens of thousands) of brain slices without any loss of the sample. The sections on the flat tape are placed on a silicon wafer, coated with a conductive material and observed with the SEM at high resolution. The ATUM-SEM has some advantages and some disadvantages. One advantage of this system is the collection of sections on a stable plastic tape, meaning that it is easy to image each sample multiple times with different resolutions. This also makes it possible to carry out immunostaining (post-embedding immuno-EM) on the tape. There are many options to increase the conductive property of the section, including carbon coating, colloidal silver, carbon double-stick tape and increased conductivity of tape, and this helps to increase the image quality by allowing the escape from unwanted charge-up. For the progress of connectomics, a

Table 2. The three major serial-EM approaches for connectomics analysis

	Automatic tape-collecting ultramicrotome scanning electron microscopy	Serial block-face scanning electron microscopy	Focused ion beam scanning electron microscopy
Abbreviations	ATUM-SEM	SBF-SEM	FIB-SEM
Sectioning performed by	Diamond knife	Diamond knife	Ion beam
Sectioning performed in	Automatic tape-collecting ultramicrotome	SEM chamber	SEM chamber
Fate of sections	Placed on the tape	Lost in chamber	Disappear
Imaging performed by	SEM	SEM	SEM
Location of tissue when imaged	Sections on the tape	Block surface	Block surface
Potential for re-observation	High	Impossible	Impossible
XY resolution	Extremely high	High	High
Z resolution	High	High	Extremely high
Size of imaged area	Wide	Moderate	Extremely narrow
Ease of three-dimensional reconstruction	Difficult	Easy	Easy
Potential for staining	Moderate	Impossible	Impossible

SEM, scanning electron microscope.

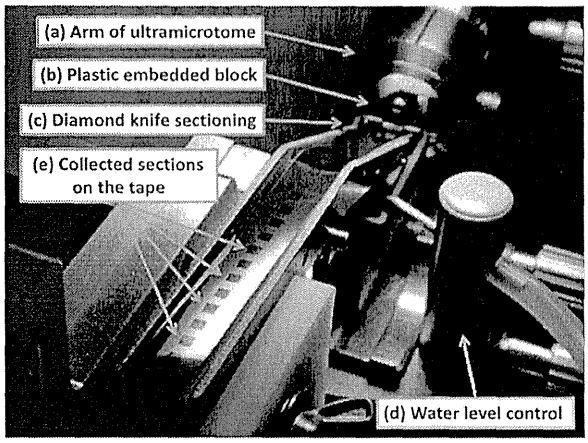

Fig. 6. A photograph of the tape collection in ATUM. The ATUM device with an ultramicrotome automatically collects serial ultrathin sections on a tape with a regular interval. The arm of the ultramicrotome (a) holds the plastic embedded tissue block (b) and makes ultrathin sections with a diamond knife (c). The system can generate several tens of thousands of sections, and the water level of the knife's water boat is automatically maintained (d). The partially submerged conveyor belt collects the ultrathin sections on to the surface of tape (e).

large area of observation is desirable. The ATUM-SEM system can be used to image an area of several square millimeters (high XY resolution), which is the largest area possible among the several serial-EM approaches. The major factors limiting the size of the imaged area are the infiltration of the fixative used for sample preparation, the maximum width of the diamond knife, the width of the collecting tape and the file size of the tiling images. The Z resolution is limited to 20–40 nm (average, 30 nm) owing to the minimum interval of the diamond-knife sectioning and the solidity of the plastic within which the brain is embedded. A disadvantage of the ATUM-SEM is the rotation of sections or unequal interval between sections on the tape, which makes it difficult to acquire sequential images automatically.

The SBF-SEM system is another SEM-based serial-EM imaging strategy used to acquire images of the top surface of microtome-sectioned plastic inside the SEM chamber [53]. Each section created with the diamond knife exposes a new surface for imaging, and thousands of sectioning repetitions create a series of surfaces for imaging. One advantage of this system is the automatic image acquisition and three-dimensional reconstruction carried out by the software built into the SEM. The possibility of the misalignment along the XY axes is limited; therefore, it is easy to find the same position in each section. This allows accurate automation of image acquisition, tiling, three-dimensional reconstruction and neural tracing. The disadvantage of the SBF-SEM system is that all sections are lost after sectioning. It is impossible to image an area of interest a second time at a different resolution, or to apply post-embedding immuno-EM to the surface of the section. There is a limited chance to enhance the conductivity of the block itself to allow the escape of unwanted charge-up. The maximum area that is possible to observe using a recent version of SBF-SEM is several 100 μm square, and this is restricted by the width of the diamond knife, the size limit of the loaded block and the maximum area that can be imaged by the microscope. The Z resolution is similar to the ATUM system; however, the thickness of the section depends on the quality of the conductive plastic within which the sample is embedded.

The third approach for serial EM is the FIB-SEM [54]. Similar to the SBF-SEM system, images are obtained from the surface of the sectioned block inside the SEM chamber. The unique characteristic of the FIB-SEM is that sectioning is carried out using a FIB, and FIB-SEM is, therefore, the best solution for studying hard tissues such as teeth and bone. The diamond knife used in the ATUM and SBF-SEM systems would not be able to cut these hard tissues smoothly and may become damaged by the tissue. An additional advantage of FIB-SEM is that the FIB can perform extremely thin sectioning (as thin as 4 nm), and the Z resolution is, therefore, higher than in the diamond-knife-sectioning approaches. The automated image acquisition and easy three-dimensional reconstruction without XY dislocation is another merit of the FIB-SEM. A disadvantage of the FIB-SEM, similar to the SBF-SEM, is the loss of the sections after sectioning, leaving no chance for re-observation or post-embedding immuno-EM and limited alternatives for enhancing the conductivity. An additional disadvantage of the FIB-SEM is that it has the smallest area of observation of all three approaches at 10 μm square area at best, even for the latest machine.

Application for LM/EM correlative analysis

In a small number of laboratories, the localization of protein or RNA is routinely visualized with different levels of resolution using both LM and EM for exactly the same sample [55–65]. This approach gives important information regarding microstructure and molecular localization in a mutually complementary manner. The combination of the serial-EM technology and the LM/EM correlative analysis that we used helps to increase the evidence for understanding physiological phenomena in future studies. It is quite important and meaningful to develop novel correlative technologies in order to connect the mapping results obtained from microscale EM and mesoscale LM.

Conclusions and perspectives

Several international connectomics projects recently began, and connectomics is attracting increasing attention. The

study of connectomics reveals the structure and function of human brain and can shed light on the mechanisms underlying neuronal diseases. The recently launched Japanese connectomics project (Brain/MINDS) aims to create a structural and functional map of the non-human primate brain by studying neural connectomics on various scales (macro, meso and micro). This project will utilize the latest technological innovations and involve international collaboration with Europe and the United States. For the structural connectomics aspect of the Brain/MINDS project, specific brain areas associated with disease in the common marmoset will be analyzed using MRI, LM and EM [1]. We hope the challenges for connectomics described here will be solved in the near future to further progress our understanding of the human brain and mind.

Acknowledgements

The authors would like to thank Dr T. Yano and Ms M. Yoshimura for their dedicated support to this project. We also thank all members of the Okano laboratory for their invaluable comments.

Funding

This work was supported by a grant-in-Aid for Scientific Research from the Ministry of Education, Culture, Sports, Science and Technology (MEXT), Japan (to S.S.), a grant from Japanese Government Scholarship program (to M.O.I.) and a grant from Brain Mapping by Integrated Neurotechnologies for Disease Studies (Brain/MINDS) supported by MEXT (to S.S. and H.O.).

References

1. Okano H, Mitra P (2014) Brain-mapping projects using the common marmoset. *Neurosci Res*. doi: 10.1016/j.neures.2014.08.014.
2. Cyranoski D (2014) Marmosets are stars of Japan's ambitious brain project. *Nature* 514: 151–152.
3. Marx V (2013) Neurobiology: brain mapping in high resolution. *Nature* 503: 147–152.
4. Hayworth K J, Morgan J L, Schalek R, Berger D R, Hildebrand D G, Lichtman J W (2014) Imaging ATUM ultrathin section libraries with WaferMapper: a multi-scale approach to EM reconstruction of neural circuits. *Frontiers Neural Circuits* 8: 68.
5. Venter J C, Adams M D, Myers E W, Li P W, Mural R J, Sutton G G, Smith H O, Yandell M, Evans C A, Holt R A, Gocayne J D, Amanatides P, Ballew R M, Huson D H, Wortman J R, Zhang Q, Kodira C D, Zheng X H, Chen L, Skupski M, Subramanian G, Thomas P D, Zhang J, Gabor Miklos G L, Nelson C, Broder S, Clark A G, Nadeau J, Mckusick V A, Zinder N, Levine A J, Roberts R J, Simon M, Slayman C, Hunkapiller M, Bolanos R, Delcher A, Dew I, Fasulo D, Flanigan M, Florea L, Halpern A, Hannenhalli S, Kravitz S, Levy S, Mobarry C, Reinert K, Remington K, Abu-Threideh J, Beasley E, Biddick K, Bonazzi V, Brandon R, Cargill M, Chandramouliswaran I, Charlab R, Chaturvedi K, Deng Z, Di Francesco V, Dunn P, Eilbeck K, Evangelista C, Gabrielian A E, Gan W, Ge W, Gong F, Gu Z, Guan P, Heiman T J, Higgins M E, Ji R R, Ke Z, Ketchum K A, Lai Z, Lei Y, Li Z, Li J, Liang Y, Lin X, Lu F, Merkulov G V, Milshina N, Moore H M, Naik A K, Narayan V A, Neelam B, Nusskern D, Rusch D B, Salzberg S, Shao W, Shue B, Sun J, Wang Z, Wang A, Wang X, Wang J, Wei M, Wides R, Xiao C, Yan C, Yao A, Ye J, Zhan M, Zhang W, Zhang H, Zhao Q, Zheng L, Zhong F, Zhong W, Zhu S, Zhao S, Gilbert D, Baumhueter S, Spier G, Carter C, Cravchik A, Woodage T, Ali F, An H, Awe A, Baldwin D, Baden H, Barnstead M, Barrow I, Beeson K, Busam D, Carver A, Center A, Cheng M L, Curry L, Danaher S, Davenport L, Desilets R, Dietz S, Dodson K, Doup L, Ferriera S, Garg N, Gluecksmann A, Hart B, Haynes J, Haynes C, Heiner C, Hladun S, Hostin D, Houck J, Howland T, Ibegwam C, Johnson J, Kalush F, Kline L, Koduru S, Love A, Mann F, May D, Mccawley S, Mcintosh T, Mcmullen I, Moy M, Moy L, Murphy B, Nelson K, Pfannkoch C, Pratts E, Puri V, Qureshi H, Reardon M, Rodriguez R, Rogers Y H, Romblad D, Ruhfel B, Scott R, Sitter C, Smallwood M, Stewart E, Strong R, Suh E, Thomas R, Tint N N, Tse S, Vech C, Wang G, Wetter J, Williams S, Williams M, Windsor S, Winn-Deen E, Wolfe K, Zaveri J, Zaveri K, Abril J F, Guigo R, Campbell M J, Sjolander K V, Karlak B, Kejariwal A, Mi H, Lazareva B, Hatton T, Narechania A, Diemer K, Muruganujan A, Guo N, Sato S, Bafna V, Istrail S, Lippert R, Schwartz R, Walenz B, Yooseph S, Allen D, Basu A, Baxendale J, Blick L, Caminha M, Carnes-Stine J, Caulk P, Chiang Y H, Coyne M, Dahlke C, Mays A, Dombroski M, Donnelly M, Ely D, Esparham S, Fosler C, Gire H, Glanowski S, Glasser K, Glodek A, Gorokhov M, Graham K, Gropman B, Harris M, Heil J, Henderson S, Hoover J, Jennings D, Jordan C, Jordan J, Kasha J, Kagan L, Kraft C, Levitsky A, Lewis M, Liu X, Lopez J, Ma D, Majoros W, Mcdaniel J, Murphy S, Newman M, Nguyen T, Nguyen N, Nodell M, Pan S, Peck J, Peterson M, Rowe W, Sanders R, Scott J, Simpson M, Smith T, Sprague A, Stockwell T, Turner R, Venter E, Wang M, Wen M, Wu D, Wu M, Xia A, Zandieh A, Zhu X (2001) The sequence of the human genome. *Science* 291: 1304–1351.
6. International Human Genome Sequencing Consortium (2004) Finishing the euchromatic sequence of the human genome. *Nature* 431: 931–945.
7. Stahnisch F W, Nitsch R (2002) Santiago Ramon y Cajal's concept of neuronal plasticity: the ambiguity lives on. *Trends Neurosci* 25: 589–591.
8. White J G, Southgate E, Thomson J N, Brenner S (1986) The structure of the nervous system of the nematode *Caenorhabditis elegans*. *Philos Trans R Soc Lond B Biol Sci* 314: 1–340.
9. Albertson D G, Thomson J N (1976) The pharynx of *Caenorhabditis elegans*. *Philos Trans R Soc Lond B Biol Sci* 275: 299–325.
10. Ward S, Thomson N, White J G, Brenner S (1975) Electron microscopical reconstruction of the anterior sensory anatomy of the nematode *Caenorhabditis elegans*. *J Comp Neurol* 160: 313–337.
11. White J G, Southgate E, Thomson J N, Brenner S (1976) The structure of the ventral nerve cord of *Caenorhabditis elegans*. *Philos Trans R Soc Lond B Biol Sci* 275: 327–348.

12. Hall D H, Russell R L (1991) The posterior nervous system of the nematode *Caenorhabditis elegans*: serial reconstruction of identified neurons and complete pattern of synaptic interactions. *J Neurosci* 11: 1–22.
13. Livet J, Weissman T A, Kang H, Draft R W, Lu J, Bennis R A, Sanes J R, Lichtman J W (2007) Transgenic strategies for combinatorial expression of fluorescent proteins in the nervous system. *Nature* 450: 56–62.
14. Feng G, Mellor R H, Bernstein M, Keller-Peck C, Nguyen Q T, Wallace M, Nerbonne J M, Lichtman J W, Sanes J R (2000) Imaging neuronal subsets in transgenic mice expressing multiple spectral variants of GFP. *Neuron* 28: 41–51.
15. Kasthuri N, Lichtman J W (2003) The role of neuronal identity in synaptic competition. *Nature* 424: 426–430.
16. Lichtman J W, Sanes J R (2003) Watching the neuromuscular junction. *J Neurocytol* 32: 767–775.
17. Walsh M K, Lichtman J W (2003) In vivo time-lapse imaging of synaptic takeover associated with naturally occurring synapse elimination. *Neuron* 37: 67–73.
18. Tabansky I, Lenarcic A, Draft R W, Loulier K, Keskin D B, Rosains J, Rivera-Feliciano J, Lichtman J W, Livet J, Stern J N, Sanes J R, Eggan K (2013) Developmental bias in cleavage-stage mouse blastomeres. *Curr Biol* 23: 21–31.
19. Loulier K, Barry R, Mahou P, Le Franc Y, Supatto W, Matho K S, Ieng S, Fouquet S, Dupin E, Benosman R, Chedotal A, Beaurepaire E, Morin X, Livet J (2014) Multiplex cell and lineage tracking with combinatorial labels. *Neuron* 81: 505–520.
20. Pan Y A, Livet J, Sanes J R, Lichtman J W, Schier A F (2011) Multicolor Brainbow imaging in zebrafish. *Cold Spring Harb Protoc* 2011: pdb.prot5546.
21. Hampel S, Chung P, Mckellar C E, Hall D, Looger L L, Simpson J H (2011) Drosophila Brainbow: a recombinase-based fluorescence labeling technique to subdivide neural expression patterns. *Nat Meth* 8: 253–259.
22. Hadjieconomou D, Rotkopf S, Alexandre C, Bell D M, Dickson B J, Salecker I (2011) Flybow: genetic multicolor cell labeling for neural circuit analysis in *Drosophila melanogaster*. *Nat Meth* 8: 260–266.
23. Lichtman J W, Livet J, Sanes J R (2008) A technicolour approach to the connectome. *Nat Rev Neurosci* 9: 417–422.
24. He Y, Chen Z J, Evans A C (2007) Small-world anatomical networks in the human brain revealed by cortical thickness from MRI. *Cereb Cortex* 17: 2407–2419.
25. Behrens T E, Sporns O (2012) Human connectomics. *Curr Opin Neurobiol* 22: 144–153.
26. Hagmann P (2005) From diffusion MRI to brain connectomics Doctoral dissertation, Institut de traitement des signaux. École Polytechnique Fédérale de Lausanne (EPFL), France. pp. 1–127. http://biblion.epfl.ch/EPFL/theses/2005/3230/EPFL_TH3230.pdf (last accessed date 3 December 2014).
27. Basser P J, Pajevic S, Pierpaoli C, Duda J, Aldroubi A (2000) In vivo fiber tractography using DT-MRI data. *Magn Reson Med* 44: 625–632.
28. Mori S, Crain B J, Chacko V P, Van Zijl P C (1999) Three-dimensional tracking of axonal projections in the brain by magnetic resonance imaging. *Ann Neurol* 45: 265–269.
29. Conturo T E, Lori N F, Cull T S, Akbudak E, Snyder A Z, Shimony J S, Mckinstry R C, Burton H, Raichle M E (1999) Tracking neuronal fiber pathways in the living human brain. *Proc Natl Acad Sci USA* 96: 10422–10427.
30. Behrens T E, Berg H J, Jbabdi S, Rushworth M F, Woolrich M W (2007) Probabilistic diffusion tractography with multiple fibre orientations: what can we gain? *Neuroimage* 34: 144–155.
31. Wedeen V J, Wang R P, Schmahmann J D, Benner T, Tseng W Y, Dai G, Pandya D N, Hagmann P, D'arceuil H, De Crespigny A J (2008) Diffusion spectrum magnetic resonance imaging (DSI) tractography of crossing fibers. *Neuroimage* 41: 1267–1277.
32. Tournier J D, Calamante F, Gadian D G, Connelly A (2004) Direct estimation of the fiber orientation density function from diffusion-weighted MRI data using spherical deconvolution. *Neuroimage* 23: 1176–1185.
33. Jansons K M, Alexander D C (2003) Persistent Angular Structure: new insights from diffusion MRI data. Dummy version. *Inf Process Med Imaging* 18: 672–683.
34. Tuch D S, Reese T G, Wiegell M R, Makris N, Belliveau J W, Wedeen V J (2002) High angular resolution diffusion imaging reveals intravoxel white matter fiber heterogeneity. *Magn Reson Med* 48: 577–582.
35. Hagmann P, Cammoun L, Gigandet X, Meuli R, Honey C J, Wedeen V J, Sporns O (2008) Mapping the structural core of human cerebral cortex. *PLoS Biol* 6: e159.
36. Irimia A, Chambers M C, Torgerson C M, Van Horn J D (2012) Circular representation of human cortical networks for subject and population-level connectomic visualization. *Neuroimage* 60: 1340–1351.
37. Irimia A, Chambers M C, Torgerson C M, Filippou M, Hovda D A, Alger J R, Gerig G, Toga A W, Vespa P M, Kikinis R, Van Horn J D (2012) Patient-tailored connectomics visualization for the assessment of white matter atrophy in traumatic brain injury. *Front Neurol* 3: 10.
38. Aggarwal M, Gobius I, Richards L J, Mori S (2014) Diffusion MR microscopy of cortical development in the mouse embryo. *Cereb Cortex*. doi: 10.1093/cercor/bhu006.
39. Ishigaki Y, Nakamura Y, Oikawa Y, Yano Y, Kuwabata S, Nakagawa H, Tomosugi N, Takegami T (2012) Observation of live ticks (*Haemaphysalis flava*) by scanning electron microscopy under high vacuum pressure. *PloS One* 7: e32676.
40. Takaku Y, Suzuki H, Ohta I, Ishii D, Muranaka Y, Shimomura M, Hariyama T (2013) A thin polymer membrane, nano-suit, enhancing survival across the continuum between air and high vacuum. *Proc Natl Acad Sci USA* 110: 7631–7635.
41. Suga M, Nishiyama H, Konyuba Y, Iwamatsu S, Watanabe Y, Yoshiura C, Ueda T, Sato C (2011) The atmospheric scanning electron microscope with open sample space observes dynamic phenomena in liquid or gas. *Ultramicroscopy* 111: 1650–1658.
42. Murai T, Maruyama Y, Mio K, Nishiyama H, Suga M, Sato C (2011) Low cholesterol triggers membrane microdomain-dependent CD44 shedding and suppresses tumor cell migration. *J Biol Chem* 286: 1999–2007.
43. Sato C, Manaka S, Nakane D, Nishiyama H, Suga M, Nishizaka T, Miyata M, Maruyama Y (2012) Rapid imaging of mycoplasma in solution using atmospheric scanning electron microscopy (ASEM). *Biochem Biophys Res Commun* 417: 1213–1218.
44. Stevens J K, Mcguire B A, Sterling P (1980) Toward a functional architecture of the retina: serial reconstruction of adjacent ganglion cells. *Science* 207: 317–319.